

(NASA-CR-170400) AN INVESTIGATION OF THE
INTERNAL AND EXTERNAL AERODYNAMICS OF CATTLE
TRUCKS Final Report (Kansas Univ. Center
for Research, Inc.) 87 p HC A05/MF A01

N83-26760

CSCL 13F G3/85

'Unclassified
03856

An Investigation of the Internal and External Aerodynamics of Cattle Trucks

Vincent U. Muirhead

Grant NAG4-8
May 1983



An Investigation of the Internal and External Aerodynamics of Cattle Trucks

Vincent U. Munhead, University of Kansas Center for Research, Inc., Lawrence, Kansas

Prepared for
Ames Research Center
Dryden Flight Research Facility
and the
U.S. Department of Agriculture
under Grant NAG-1-8



National Aeronautics and
Space Administration
Ames Research Center
Dryden Flight Research Facility
Edwards, California 93523



U.S. Department of Agriculture
Agriculture Research Service
El Reno, Oklahoma 73036

TABLE OF CONTENTS

	<u>Page</u>
TABLE OF CONTENTS.....	i
LIST OF SYMBOLS.....	ii
LIST OF FIGURES.....	iv
LIST OF TABLES.....	vii
ACKNOWLEDGEMENTS.....	viii
SUMMARY.....	ix
1. INTRODUCTION.....	1
2. APPARATUS AND PROCEDURE.....	3
2.1 Models.....	3
2.2 Mounting.....	4
2.3 Tests.....	5
3. RESULTS AND DISCUSSION.....	5
3.1 Internal Trailer Airflow Patterns.....	5
3.2 Internal Trailer Airflow Speeds.....	8
3.3 Melting Times for Ice Cubes in Trailer.....	11
3.4 Drag Coefficients and Power Required.....	11
3.5 Side Force Coefficients.....	13
3.6 Lift and Moment Coefficients.....	14
4. CONCLUSIONS AND RECOMMENDATIONS.....	14
5. REFERENCES.....	16
6. FIGURES AND TABLES.....	17
7. APPENDIX.....	75

LIST OF SYMBOLS

<u>Symbol</u>	<u>Definition</u>
A	Projected model frontal area (less wheels) on a plane perpendicular to the centerline of vehicle, .0915 sq m (.986 sq ft)
A_b	Base area at the aft end of livestock trailer
A_{bv}	Total area of vent openings in base of trailer
A_s	Total side area of trailer (one side)
A_{sv}	Total area of slotted openings on one side of trailer
A_i	Total area of ram-air inlet or NACA submerged inlets, normal to longitudinal axis of model
A_m	Total area of manifold ducting openings at the front wall of the livestock compartment
C_D	Coefficient of drag, D/qA
C_L	Coefficient of lift, L/qA
C_M	Coefficient of pitching moment, PM/qAc
C_Y	Coefficient of side force, SF/qA
C_R	Coefficient of rolling moment, RM/qAc
C_N	Coefficient of yawing moment, YM/qAc
C_{D_X}	Coefficient of drag, configuration X
C_p	Coefficient of static pressure, $(P - P_A)/q$
c	Reference length (vehicle length for C_M) (vehicle width for C_R , C_N)
D	Drag (vehicle axis)
D_e	Equivalent diameter, $\sqrt{4A/\pi}$
L	Lift (vehicle axis)
P	Power
P_A	Atmospheric pressure

<u>Symbol</u>	<u>Definition</u>
P'	Local static pressure
PM	Pitching moment (vehicle axis)
q	True dynamic pressure in wind tunnel test section, $1/2\rho v^2$
RM	Rolling moment (vehicle axis)
R_N	Reynolds number (based on equivalent diameter, $\frac{\rho V D}{\mu}$)
SF	Side force (vehicle axis)
V	Relative wind speed = Wind tunnel airspeed
v_1	Vehicle speed
v_2	Side wind component
w	True wind speed
YM	Yawing moment (vehicle axis)
β	Wind angle relative to vehicle path
ρ	Air density
μ	Air viscosity
ψ	Yaw angle = Relative wind angle

LIST OF FIGURES

<u>Number</u>	<u>Title</u>	<u>Page</u>
2.1.1	Photograph of baseline wind tunnel model, configuration 1.....	18
2.1.2	Baseline wind tunnel model, configuration 1.....	19
2.1.3	Pressure tap locations in baseline trailer model, configuration 1, sides and decks.....	20
2.1.4	Pressure tap locations in baseline trailer model, configuration 1, front and rear.....	21
2.1.5	Tuft locations in trailer models, 2, 5, and 6.....	22
2.1.6	Airspeed measurement locations in trailer models 2, 5, and 6.....	23
2.1.7	Ice cube locations in trailer models 2, 5, and 6 for ice cube melting tests.....	24
2.1.8	Side view of streamline wind tunnel models.....	25
2.1.9	Forward streamlining, full scale, as in reference 8, 10, and 13.....	26
2.1.10	Photograph of forward streamlining and ram air inlet on configuration 5.....	27
2.1.11	Ram air inlet and ducting design applied to configuration 5.....	28
2.1.12	NACA submerged inlet and ducting design applied to configuration 6.....	29
2.1.13	Cattle simulation design.....	30
2.1.14	Model configuration chart.....	31
2.1.15	Important Physical Proportions for models.....	32
3.1.1	Air flow in trailer $\psi = 0^0$, configuration 1, isometric view indicating air flow direction only.....	33
3.1.2	Air flow in trailer, $\psi = 0^0$, configuration 1, upper and rear decks.....	34
3.1.3	Air flow in trailer, $\psi = 0^0$, configuration 1, lower deck.....	35
3.1.4	Air flow in trailer, $\psi = 15^0$ configuration 1, isometric view indicating air flow direction only.....	36

3.1.5	Air flow in trailer, $\psi = 15^0$, configuration 1, upper and rear decks.....	37
3.1.6	Air flow in trailer, $\psi = 15^0$, configuration 1, lower deck.....	38
3.1.7	Photograph of tufts in trailer, configuration 1, $\psi = 0^0$	39
3.1.8	Air flow in trailer, $\psi = 0^0$, configuration 2, upper deck above cattle.....	40
3.1.9	Air flow in trailer, $\psi = 0^0$, configuration 2, upper deck below cattle.....	41
3.1.10	Air flow in trailer, $\psi = 0^0$, configuration 2, lower and rear decks above cattle.....	42
3.1.11	Air flow in trailer, $\psi = 0^0$, configuration 2, lower and rear decks below cattle.....	43
3.1.12	Air flow in trailer, $\psi = 15^0$, configuration 2, upper deck above cattle.....	44
3.1.13	Air flow in trailer, $\psi = 15^0$, configuration 2, upper deck below cattle.....	45
3.1.14	Air flow in trailer, $\psi = 15^0$, configuration 2, lower and rear decks above cattle.....	46
3.1.15	Air flow in trailer, $\psi = 15^0$, configuration 2, lower and rear decks below cattle.....	47
3.1.16	Air flow in trailer, $\psi = 0^0$, configuration 5.....	48
3.1.17	Air flow in trailer, $\psi = 15^0$, configuration 5.....	49
3.1.18	Air flow in trailer, $\psi = 0^0$, configuration 6.....	50
3.1.19	Air flow in trailer, $\psi = 15^0$, configuration 6.....	51
3.4.1	Reynolds number effect on drag coefficient, configuration 1.....	52
3.4.2	Effect of relative wind angle on drag coefficient, configuration 1.....	53
3.4.3	Effect of relative wind angle on drag coefficient, configuration 3.....	54
3.4.4	Effect of relative wind angle on drag coefficient, configuration 4.....	55

3.4.5	Comparison of drag coefficients, configurations 1, 3, 4.....	56
3.4.6	Power required to overcome aerodynamic drag, configurations 1, 3, 4.....	57
3.5.1	Reynolds number effect on side force coefficient, configuration 1.....	58
3.5.2	Effect of relative wind angle on side force coefficient, configuration 1.....	59
3.5.3	Comparison of side force coefficients, Configura- tion 1, 3, 4.....	60
3.6.1	Effect of relative wind angle on lift coefficients, Configuration 1.....	61
3.6.2	Comparison of lift coefficients, Configurations 1, 3, 4.....	62

LIST OF TABLES

<u>Number</u>	<u>Title</u>	<u>Page</u>
I	Coefficients of Static Pressure, Configuration 1.....	63
II	Internal Air Flow Speeds, Configuration 2.....	67
III	Internal Air Flow Speeds, Configuration 5.....	68
IV	Internal Air Flow Speeds, Configuration 6.....	69
V	Internal Air Flow Volumes for Models.....	70
VI	Melting Times for Ice Cubes from Internal Air Flow, Configuration 2.....	71
VII	Melting Times for Ice Cubes from Internal Air Flow, Configuration 5.....	71
VIII	Melting Times for Ice Cubes from Internal Air Flow, Configuration 6.....	72
IX	Drag Coefficients.....	72
X	Potential Fuel and Economic Savings of Modified Vehicles Relative to Configurations 1 and 2.....	73
XI	Side Force Coefficients, $R_N = 7 \times 10^5$	73
XII	Lift Coefficients, $R_N = 7 \times 10^5$	73
XIII	Pitching Moment Coefficients, $R_N = 7 \times 10^5$	74
XIV	Rolling Moment Coefficients, $R_N = 7 \times 10^5$	74
XV	Yawing Moment Coefficients, $R_N = 7 \times 10^5$	74

ACKNOWLEDGMENTS.

The advice and comments of Mr. Edwin Saltzman, NASA Dryden Flight Research Facility, are gratefully acknowledged. The wind tunnel testing and data reduction were conducted by the following students in the Department of Aerospace Engineering, University of Kansas:

Jay Brandon, Graduate student

Carlos Blacklock, Undergraduate student

Michael Owings, Undergraduate student

Sheryl Scott, Undergraduate student

1.0 INTRODUCTION

The environmental conditions which exist during the transit of livestock greatly affect the shrinkage which the animals undergo and the quality of the meat when slaughtered. Although the problems associated with the mass transit of livestock are similar to those associated with the transit of humans, the problems encountered with livestock are much greater because of "the greater heat production per animal, the proportion of latent heat (evaporative) to the total heat, higher animal loading density and management factors."¹ Large volumes of heat and metabolic byproducts must be removed.

Some of the factors which effect shrinkage and meat quality are:¹⁻⁵

1. Air temperature in hauler
2. Air movement in hauler
3. Humidity in hauler
4. Wind chill in hauler
5. Distance and time in transit
6. Exposure to dust, smoke, snow, rain, hail, wind
7. Degree of excitement in transit
8. Space per animal
9. Initial body weight
10. Kind of animal, species

Under good conditions the shrinkage may vary from 1% to 8% in present vehicles. Freezing rain and low temperatures, or high temperatures and humidity can be deadly. The effect of long-term preslaughter stress such as occurs in transit depletes muscle glycogene. This results in dryer meat with a darker color and a higher pH.²

Special efforts have been made to control the environment for disease-exposed cattle during transit⁵ and in the air shipment of livestock.¹ Efforts have been made (by J. H. Thorne & Sons, Ltd., Shropshire, England, and in Denmark) to improve air flow in haulers for pigs. A venting system for a double deck standard truck was patented by H. L. McGan.⁶ Recently a patent has been granted for a streamline livestock hauler concept with a venting system to improve internal flow conditions.⁷

During the past decade considerable research has been conducted to reduce the aerodynamic drag on tractor trailer vehicles, smaller two-axle trucks, recreation vehicles and automobiles. These vehicles have been closed van type cargo vehicles, without side venting such as livestock trucks conventionally have. This research has shown that a significant reduction in aerodynamic drag can be achieved by the proper streamlining,⁸⁻¹³ thereby reducing fuel consumption considerably.

Most vehicles used to transport livestock have numerous small openings along the sides for ventilation and they usually have solid, i.e., unvented, walls at the front and rear of the livestock compartment. This arrangement generally increases the aerodynamic drag and, of more importance, presents an uncontrolled environment in the cargo compartment, i.e., poor ventilation for the animals. This environment subjects the animals to:

1. various wide ranging and uncontrolled localized air flow speeds and directions
2. various and uncontrolled amounts of exhaust fumes, dust particles, rain, sleet and snow
3. local pooling of poor quality air due to poor flushing capability
4. local severe turbulence conditions due to vortices
5. a variety of uncontrolled temperatures and humidity conditions.

Thus, it would appear that by the proper aerodynamic design of the vehicle the environment for the animals can be greatly improved and the aerodynamic drag reduced.

Wind tunnel tests have been conducted at the University of Kansas on a one-tenth scale model of a conventional tractor trailer cattle hauler (empty) to determine the air flow patterns through the trailer and the drag of the vehicle. These results were used as a baseline for comparison with results of tests on subsequent modifications which were made to the baseline vehicle. The modifications reported herein are:

1. baseline model with a full loading of simulated cattle,
2. baseline model with smooth sides,
3. baseline model with smooth sides and streamlining,

4. streamline model with two forebody modifications and vented base region intended to provide improved ventilation in the livestock trailer (and had the smooth sides as in item 3, above).

2.0 APPARATUS AND PROCEDURE

2.1 Models

The baseline wind tunnel model, Configuration 1, is shown in Figures 2.1.1 through 2.1.4. It is a one-tenth scale model of a geometrically representative cattle trailer and a cab-over-engine tractor. The structural base of the model was constructed of steel and was mounted on the wind tunnel balance with two support struts. The tractor cab was constructed of fiberglass and mounted on the structural base. The trailer sides, top and intermediate floor were constructed from Plexiglass; the front and rear ends were made of wood. Wooden supports were mounted on steel rods attached to the structural base.

The important geometric features of current cattle-truck trailer design were closely simulated, including: scaled external dimensions; side panels and open slots, including a representative overall ratio of slotted area to total side panel area and the vertical and longitudinal distribution of the openings; vertical posts; and internal floors and bulkheads. The wall and floor thicknesses were not scaled. The major features of the cab were also closely simulated, but details were omitted. Figures 2.1.5 through 2.1.7 show the location of tufts, air speed probes and ice cube melt points in the trailer models. The melting times of small ice cubes which were placed at these points were used as indicators of the relative local ventilation characteristics.

The streamline tractor trailer model (without provisions for ingesting ventilation air) is shown in Figure 2.1.8. This is the same basic shape, except for the "dropped" mid region of the trailer, as tested in the wind tunnel and reported in references 8 and 13, and as tested in full scale, references 10 and 13. Details of the forebody geometry at full scale are shown in Figure 2.1.9.

Figures 2.1.10 and 2.1.11 show features of models having the forebody geometric proportions of the previous two figures combined with ram air inlets for providing positive ventilation for the cargo compartment.

ment. A configuration which uses the NACA submerged inlet concept is shown in Figure 2.1.12.

Simulated cattle were used in configurations 2, 4, 5 and 6. These were simulated by using modified rectangular styrofoam blocks to represent the cattle bodies. The blocks were notched at the top, bottom and each side to simulate a closely packed loading. Wooden dowls were used to simulate the legs supporting the simulated bodies. These features are shown in Figure 2.1.13. A configuration chart, Figure 2.1.14, shows a summary list of the model configurations tested. It is important to notice in figure 2.1.14 that whereas configurations 5 and 6 had solid (i.e., unvented) side walls for the livestock compartment, these were the only configurations having vents in the base region. A listing of important inlet and exit ventilation areas is given in Figure 2.1.15.

2.2 Mounting

The models were mounted directly on two supports on the wind tunnel balance, Figure 2.1.2, so that the wheels of the model were approximately .794 cm (.313") above the floor of the wind tunnel. This is not the usual arrangement for mounting a truck model. Because of the relatively large size of the model, with respect to the test section, there wasn't sufficient space for a conventional ground board. While this was a less than optimum arrangement for measuring forces, the larger model was deemed to be important to enhance the internal pressure, flow direction and air speed measurements which would have been more difficult to define within a smaller model.

The flow over the model was observed from either side of the test section and from above the test section. The model could be rotated 20° in each direction from the centerline of the wind tunnel. A nozzle to emit neutrally buoyant helium bubbles was mounted in a traversing mechanism upstream of the test section (the helium bubbles provided a visual indication of flow patterns). This enabled the positioning of the bubble stream at varying heights along the vehicle, varying locations across the front of the vehicle and at various distances from the tractor and/or trailer. The bubbles were illuminated by two zenon

lights downstream of the models as well as flood lighting in the test section area.

2.3 Tests

The tests were conducted in the .91 by 1.29 meter wind tunnel at the University of Kansas at Reynolds numbers of 2.5×10^5 to 10.1×10^5 based upon the equivalent diameter of the vehicle or 1.27×10^6 to 5.15×10^6 based upon the length of the baseline model. The Reynolds number was controlled by adjusting the wind tunnel airspeed from 40.5 to 159.5 kilometers per hour (25.2 to 99.1 mph). Tests were made at yaw (relative wind) angles of 0°, 5°, 10°, and 15° at four different Reynolds numbers. Force and moment data were obtained from a six-component, strain-gauged balance. Pressure measurements were made by an alcohol manometer. A Sage Action, Inc., neutrally buoyant helium bubble system and tufts were used to visualize the air flow inside the trailer and around the entire model. The bubble flow and tufts were visually observed and manually recorded as well as photographed with a 35 mm camera.

Probes were placed inside the trailer model to measure air speeds in each section of the trailer. Ice cubes (volume of 1.96 ml) each were placed inside the trailer to obtain a relative melt time interval from the air flow in configurations 2, 5 and 6. During each test one cube was placed on the top of the trailer in quasi-free stream flow in order to provide a reference for correlating the numerous tests.

3.0 RESULTS AND DISCUSSION

3.1 Internal Trailer Air Flow Patterns

3.1.1 Baseline Model, Configuration 1.

The internal air flow in the trailer of the baseline model (without simulated cattle) is illustrated in Figures 3.1.1 through 3.1.7. These illustrations are a composite of manually recorded visual observations and photographs of both helium bubble flow and tuft patterns. Three intensities of lines are used in Figures 3.1.2, 3.1.3, 3.1.5 and 3.1.6 in order to provide some understanding of the flow speeds in the trailer. These intensities were established from the observed bubble flow speed, the tuft activity level and pressure measurements. The

pressure coefficients in Table I (exterior and interior) were calculated from local static pressures measured on the surfaces of the trailer. The air flow in the trailer was turbulent and the head losses unknown. Therefore, the coefficients do not reflect the true local airspeeds. The coefficients were used to assist in establishing quantitatively the relative speed scales on each of the flow illustrations.

At a relative wind angle of $\psi = 0^\circ$, the air flowing over the cab and trailer entered the trailer in the forward and central region, Figures 3.1.2 and 3.1.3. The air entered on the right (starboard) side and exited along the left (port) side. This was caused by a flow angularity of less than one degree and small variations from symmetry of the cab. The highest air flow speeds and the strongest vortices occurred in the forward portions of the upper and lower deck areas. The air flow speeds diminished in the aft regions of the trailer.

At relative wind angles of $\psi = 5^\circ$ and 10° , not shown herein, and 15° , Figures 3.1.4 through 3.1.6, the air entered the trailer over the forward half of the trailer on the right (windward) side of the trailer and exited on the left (leeward) side. As the relative wind angle increased, the internal air flow speeds progressively increased in the forward part of the trailer with the flow patterns remaining similar, Figures 3.1.4, 3.1.5 and 3.1.6. The airflow in the rear deck area of the trailer became negligible at $\psi = 10^\circ$ and $\psi = 15^\circ$ relative wind angles.

Generally the internal flow for the empty trailer was characterized by turbulence, vorticity and some forward flow in the upper and lower deck areas. In the rear deck of the trailer there was very little air movement. Also from the general flow conditions it would appear that dust, smoke particles or other impurities entering the trailer would be most concentrated in the forward part of the trailer. In all cases the conditions which existed within the trailer varied as a function of the relative wind speed and direction.

3.1.2 Baseline Model with Simulated Cattle, Configuration 2.

The internal flow in the trailer with a load of simulated cattle is illustrated in Figures 3.1.8 through 3.1.15. These illustrations were made from visual observations of tufts placed inside the trailer. The

blockage caused by the cattle produced two main changes in the flow pattern of the empty tractor: 1) the internal flows were weaker, and 2) the flow patterns were less turbulent. In general, and not surprisingly, it would appear that the denser the loading of the tractor, the weaker the air flow.

Livestock in the front of the upper and lower decks will be subject to a greater concentration of foraging particles. Though these simulated effects of livestock on internal flow patterns do not provide comprehensive quantitative data it is evident that follow-on experiments should include the effects of normal livestock loading densities.

3.1.3 Streamline Model with Ram Air Inlet and Ducting, Configuration 5

The streamline tractor tractor model, Configuration 5, contained a load of simulated cattle. The ram air inlet and ducting were designed to produce an air flow from front to rear and of approximately the same speed above and below the simulated cattle in each compartment. As illustrated in Figures 3.1.16 and 3.1.17, the air flow pattern was from front to rear and in each deck area was nearly independent of yaw angle.

3.1.4 Streamline Model with NACA Submerged Inlets and Ducting, Configuration 6.

The streamline tractor tractor model, configuration 6, contained a load of simulated cattle. The ram air inlet and duct system of configuration 5 was replaced by four NACA submerged inlets on each side of the vehicle in the gap between the cab and the tractor, so that one unit on each side was located above or below the simulated cattle on both the upper and lower decks. Air from the inlet on top flowed above the simulated cattle on the upper deck. The general air flow for configuration 6 at relative wind angles of 0° and 5° (only data for $\psi = 0$ shown) is illustrated in Figure 3.1.18. The flow was from front to rear. However, at relative wind angles of 10° and 15° reverse flow occurred on the left (leeward) side, Figure 3.1.19. Most of the air entered the front of the tractor through the right (windward) side inlets. A very small amount of air entered through the left (leeward) inlets.

3.2 Internal Trailer Air Flow Speeds

3.2.1 Baseline Model with Simulated Cattle, Configuration 2.

The internal air flow speeds for configuration 2 at the locations shown in Figure 2.1.6 are given in Table II. Considerable forward flow occurred for all wind angles, the location and speeds varying with wind angle. Measured speeds varied from a positive value of 24.9m/sec (81.7 ft/sec), about 75% of free stream velocity, to a negative value of 8.4m/sec (27.6 ft/sec). Local speeds at these points may have been greater than the table values since the pitot tubes were placed parallel to the fore and aft axis of the trailer and no attempt was made to determine the flow angularity from this axis. However, tufts at the measurement points indicated general forward or aft flow as indicated by the signs in Table II. Using the average wind speeds in the upper and lower decks, a volume air flow was calculated and is given in Table V. It will be noted that the total volume of flow is very dependent upon the relative wind angle for configuration 2.

3.2.2 Streamline Model with Ram Air Inlet and Ducting, Configuration 5.

The internal air flow speeds for configuration 5 are given in Table III. At each measurement point the air flow is from forward to aft at all angles of relative wind. Although individual speeds vary from a maximum of 6.2m/sec (20.5 ft/sec) to a minimum of 2.0m/sec (6.5 ft/sec), the average speeds at each location, A, B, C, etc., vary only from 4.90m/sec (16.1 ft/sec) to 2.71m/sec (8.5 ft/sec). The lowest overall average values occur at location D. It will be noted that the air flowing into this region flows through smaller entrance holes in the trailer, and through a much more devious path, see Figures 2.1.6 and 2.1.11. The smaller entrance holes were necessitated by the initial model design and could be corrected by redesign. Using the average wind speeds in the upper and lower decks, the volume flow through the trailer was calculated. In contrast to the data from configuration 2, Table V shows that the resulting volume of flow for configuration 5 is nearly independent of relative wind direction.

Reference 1 indicates that $1.70 \text{ m}^3/\text{min}$ (60 cuft/min.) of air (maximum) is required per 45.5 kilograms (100 pounds) weight of cattle for on-ground

ORIGINAL PAGE IS
OF POOR QUALITY

situations during air shipment. This ventilation rate, i.e., the fresh air supplied from outside, provides for oxygen requirements, heat removal, odor removal and water vapor removal. Using this figure for a full load of cattle (42 animals at 1100 pounds each), $784 \text{ m}^3/\text{min}$. ($27,720 \text{ cuft/min.}$) of air flow is required. Based upon the data from Tables III and V, this amount of air would flow through the trailer for a full-scale configuration 5 at a vehicle speed of approximately 95.3 km/hr (59.2 mph).*

At the low Reynolds numbers of these model tests the boundary layer is disproportionately thicker than would occur on a full-scale version of configuration 5. This makes the model inlet and ducting operate as if it were smaller than it actually is. Thus it is believed that a full-scale prototype of configuration 5 would provide greater amounts of internal air flow at any given speed than predicted from the model; and that the required amount of air flow could be obtained at vehicle speeds significantly below those stated in the previous paragraph. Furthermore, the present ram-air inlet to trailer side area ratio is 2.0 percent for model configuration No. 5. If the mass-flow of air desired is greater than a full-scale version of configuration 5 can achieve, then the ram-air inlet area can be increased for the final design.

At or near zero speed, fans would be required. Using a fan at each of eight .46 m (1.5 ft) diameter air entrances at the front of the trailer, $1024.6 \text{ m}^3/\text{min}$ ($36,240 \text{ cuft/min}$) of air could be introduced into the trailer through the ram air inlet and ducting with no forward motion of the vehicle. Thus, with fans and dampers the air flow into the trailer could be completely controlled to provide whatever amount was optimal. In addition, the air could be heated or cooled as desired to provide a controlled livestock environment. A water trap would capture precipitation.

3.2.3 Streamline Model with NACA Submerged Inlets and Ducting, Configuration 6.

The internal air flow speeds for Configuration 6 are given in Table IV. With exception of the left side of the lower and rear decks at

*A reference 1 author recently stated that revised maximum air flow needs may be about 1/3 of the reference 1 values. Thus configuration 5 would provide ample air flow at relatively low vehicle speeds, and the next paragraph may become an academic matter.

**ORIGINAL PAGE IS
OF POOR QUALITY**

angles of relative wind of 10° and 15°, all air flow was from forward to aft. The flow speeds varied from a maximum of 4.0m/sec (13.0 ft/sec) to a minimum of -2.8m/sec (-9.1 ft/sec). The volume flow, Table V, was influenced more by relative wind angle than was the volume flow in configuration 5. The volume flow was also much less than in configuration 5. The average volume flow over the 15° angle of yaw was only 40.7% of the average volume flow for configuration 5.

The total inlet area for the nine NACA submerged inlets was only about 18% of the ram air inlet of configuration 5, Figure 2.1.15. Thus, a comparison of the ventilation characteristics for configurations 5 and 6 is not very realistic in that the latter configuration was denied a competitive total inlet area. However, the rear exit area (A_{bv}) was the same for both. Furthermore, it is believed that the 1/10 scale truck model was too small to maintain the proper boundary layer thickness to submerged inlet dimensional scaling proportions*, thereby impeding the efficiency of each individual submerged inlet. All-in-all it is surprising that the air flow characteristics of configuration 6 appear as favorable as they do, and it may be that, based upon the present results, submerged inlets should not be disqualified as a candidate means of providing high quality air flow in ample quantities.

Thus, it may be practical to increase the size of the submerged type inlets to achieve more inlet area; and perhaps the number of such inlets could also be increased. However, at low vehicle speed it would be more difficult to provide the required air with fans as compared with configuration 5. Also, if it were desired to cool or heat the air this would be more difficult than with configuration 5.

The right (windward) side inlets provide most of the air going into the trailer. This causes the reverse internal flow at the higher relative wind angles. It appears that these inlets would also entrap smoke, dust and other foreign materials much more than the ram air inlet of configuration 5.

*It is well known in wind-tunnel testing that at low Reynolds numbers the boundary layer on the small scale model can be disproportionately too thick for the size of the test specimen.

3.3 Melting Times for Ice Cubes in Trailer

In order to provide some quantitative measure of the wind effect and the ventilation characteristics of each configuration, ice cubes (volume of 1.96 ml each) were placed at the points indicated in Figure 2.1.7. The tunnel was operated at a constant speed of 33.5 m/sec (110 ft/sec) until all cubes were melted. Since the tunnel temperature could not be maintained constant, one "reference" cube was placed on the top of the trailer in quasi-free stream flow to provide a means of obtaining a correction factor. All data were corrected to a tunnel reference temperature of 26.7°C (80°F).

The time of melting for the ice cubes varied from 1.6 to 14.3 minutes for configuration 2, from 3.4 to 19.0 minutes for configuration 5 and from 6.3 to 26.5 minutes for configuration 6. The relative low values for configuration 2 reflect the very high local air speeds existing in parts of the cargo areas. The streamline vehicles have relatively longer melting times which reflect the slower and more evenly distributed flow.

3.4 Drag Coefficients and Power Required

Drag coefficients were computed from the force acting on the wind tunnel model along the model axis. The reference area used was the projected frontal area (A). The drag coefficients were plotted as a function of Reynolds number for each of several yaw angles and the values for configuration 1 are shown in Figure 3.4.1. A Reynolds number of 7×10^5 (based upon equivalent diameter) was selected to compare the drag data of various configurations in this test series. Figures 3.4.2 through 3.4.5 show the effect of relative wind angle on configurations 1, 3 and 4. Table IX presents the data for these three configurations and a comparison with test data of configurations 1, 4 and 5 of reference 8.

In spite of model and mounting variations between configuration 3 of this series of tests and the baseline model, configuration 1 of reference 8, the drag coefficients compare reasonably well. At a relative wind angle of $\psi = 0^\circ$, configuration 3 presented much the same profile to the air as did configuration 1 of references 8 or 9. For the present tests the lower portion of the vehicle was in the boundary layer

of the test section floor which would contribute to the drag coefficient of the present configuration 3 being 17.6% less than configuration 1 of reference 8. As the relative wind angles increased, the drag of configuration 3 exceeded that of configuration 1 of references 8 or 9. This increase can be attributed mainly to model differences such as greater side area of the cattle trailer, differences in wheel dimensions, other small parts not detailed as well and a different wind tunnel mounting. Thus, the profile to the air was somewhat different than configuration 1 of references 8 or 9 and the profile differences increased with increasing values of yaw angle.

At relative wind angles of 0° and 5° the drag coefficients of configuration 4 compare closely with those of the streamlined configuration 4 of reference 8, Figure 3.4.4. At angles of 10° and 15° the air profile differences of configuration 4, of the present tests, increased the drag coefficients above those of configuration 4 of reference 8.

Considering now only the configurations of the present test series, at all relative wind angles, configuration 1 with slotted sides had a higher drag coefficient than the smooth sided configuration 3. The average drag coefficient of configuration 3, 1.55, over the 15° relative wind range was 15.8% less than configuration 1. The streamline model, configuration 4, had a lower drag coefficient at all relative wind angles than either configuration 1 or 3. The average drag coefficient of 1.109 over the 15° relative wind range was 39.7% less than configuration 1 and 28.5% less than the average drag coefficient of configuration 3.

Tests were made on the drag of configuration 2, 5 and 6 which are not reported herein. These tests indicated that a full complement of simulated cattle in configuration 2 decreased the drag slightly from the empty condition of configuration 1. Likewise the venting of the trailer with the ram air inlet, configuration 5, or the NACA submerged inlets, configuration 6 (each in combination with the vented base region) decreased the drag slightly from the no internal flow condition of configuration 4. These differences (all differences discussed in this paragraph) were generally less than 1%.

The power required to overcome the aerodynamic drag of configurations 1, 3 and 4 has been calculated for a vehicle ground speed of 88.5 Km/hr (55 mph) and for the annual nationwide average wind speed for the United States of 15.3 Km/hr (9.5 mph). Figure 3.4.6 shows the variation of power required to overcome aerodynamic drag for these configurations at full scale as the wind direction varied from a head wind, $\beta = 0^\circ$, around to a tail wind, $\beta = 180^\circ$. Because of the similarity of the drag for configurations 1 and 2 (and the corresponding similarity for configurations 4, 5, and 6) as described in the previous paragraph, the power required values calculated for configuration 1 apply to 2, and values for configuration 4 also apply for configurations 5 and 6.

These power-required values have been used to calculate the potential savings in fuel for configurations 3, 4, 5 and 6 relative to configurations 1 and 2. These incremental savings will show the effects of slotted versus smooth trailer sides and the influence of streamlining, respectively. For these computations a normal brake specific fuel consumption of 2.129×10^{-4} Kg of fuel per watt-hour (.35 pounds per horsepower-hour) was used.⁸ The fuel density was assumed to be .834 Kg/liter (6.96 lb/gal). The fuel cost was assumed to be .64 cents per liter (1 dollar per gallon). Based upon these assumptions, the hourly fuel savings and the savings based upon 160,900 Km (100,000 mi) of operation was calculated. The potential fuel savings per hour of configuration 4, 5 or 6 over configuration 1 or 2 was 17.2 liters/hour (4.5 gal/hr) or \$4.53 cost savings per hour. On the basis of 160,900 Km (100,000 mi) of vehicle mileage the fuel saving was 31,190 liters (8,240 gal.) or a cost savings of \$8,240, Table X.

3.5 Side Force Coefficients

The side force coefficients are given in Table XI. Figure 3.5.1 shows the variation of side force coefficients for configuration 1 with Reynolds number. Figure 3.5.2 shows the variation of side force coefficients with relative wind angle for a Reynolds number of 7×10^5 . These values were used to normalize the corresponding side force data for the other configurations for Figure 3.5.3. Both the smooth (unslotted) trailer sides and the cab and gap fairing increased the side force coefficient at all yaw angles tested.

3.6 Lift and Moment Coefficients

The lift and moment coefficients are not of direct interest in this investigation, but are included for completeness and possible future interests in vehicle stability and control. The variation of lift coefficients with relative wind for configuration 1 is given in Figure 3.6.1. Table XII contains the lift coefficients for configuration 1, 3 and 4. A comparison of these lift coefficients is given in Figure 3.6.2.

The moment coefficients are contained in Tables XIII, XIV and XV. The moments were taken about a point on the centerline of the vehicle 106.3 cm (41.9") from the front of the vehicle and 35.6 cm (14.0") above ground level. The reference area used was the projected frontal area (A); the reference length (c) for the pitching moment was the vehicle length; the reference length (c) for the rolling and yawing moments was the vehicle width. The rolling and yawing moments were corrected for flow angularity.

4.0 CONCLUSIONS AND RECOMMENDATIONS

The following conclusions can be drawn from the tests conducted.

1. The airflow in the subscale model of a representative commercial livestock trailer was indeed random and variable. There were conditions wherein there was virtually stagnant air in some locations and very rapid air flow (up to 75% of free stream velocity) in other locations of the cargo compartment. The local internal flow conditions were very dependent on the relative wind angle.

2. The streamlined configuration with a ram air inlet and ducting, vented base and fans can provide a nearly uniform air flow throughout the trailer under conditions of variable wind angles, wind speeds and vehicle speeds (including while the vehicle is not in motion). This air flow could be adjusted to provide the most desirable flow conditions for the cattle. Further, as desired, the incoming air could be heated or cooled and precipitation extracted.

3. The streamline configuration with NACs submerged inlets and vented base could provide better flow conditions than the subscale model of the representative commercial trailer. It would be more difficult to provide the proper air flow at low vehicle speeds, to heat or cool the

air and to remove precipitation with the NACA submerged inlets than with the ram air inlet configuration. Additionally the air coming in the side ducts would probably be more likely to contain dust, smoke and other impurities.

4. The streamline vehicles present a significant potential fuel saving of approximately \$8,240 per 160,900 Km (100,000 mi) of operation.

It is recommended that a series of full-scale tests be conducted on a prototype vehicle based upon the configuration 5 design to:

1. Establish the appropriate internal flow rates for different temperature and loading conditions which are most desirable for various kinds of animals during transit.

2. Establish environmental criteria for the design of future livestock haulers.

3. Define statistically significant livestock and economic losses experienced with representative conventional haulers as compared to prototype haulers having design based primarily on configuration 5.

4. Check the validity of the wind tunnel results.

5.0 REFERENCES

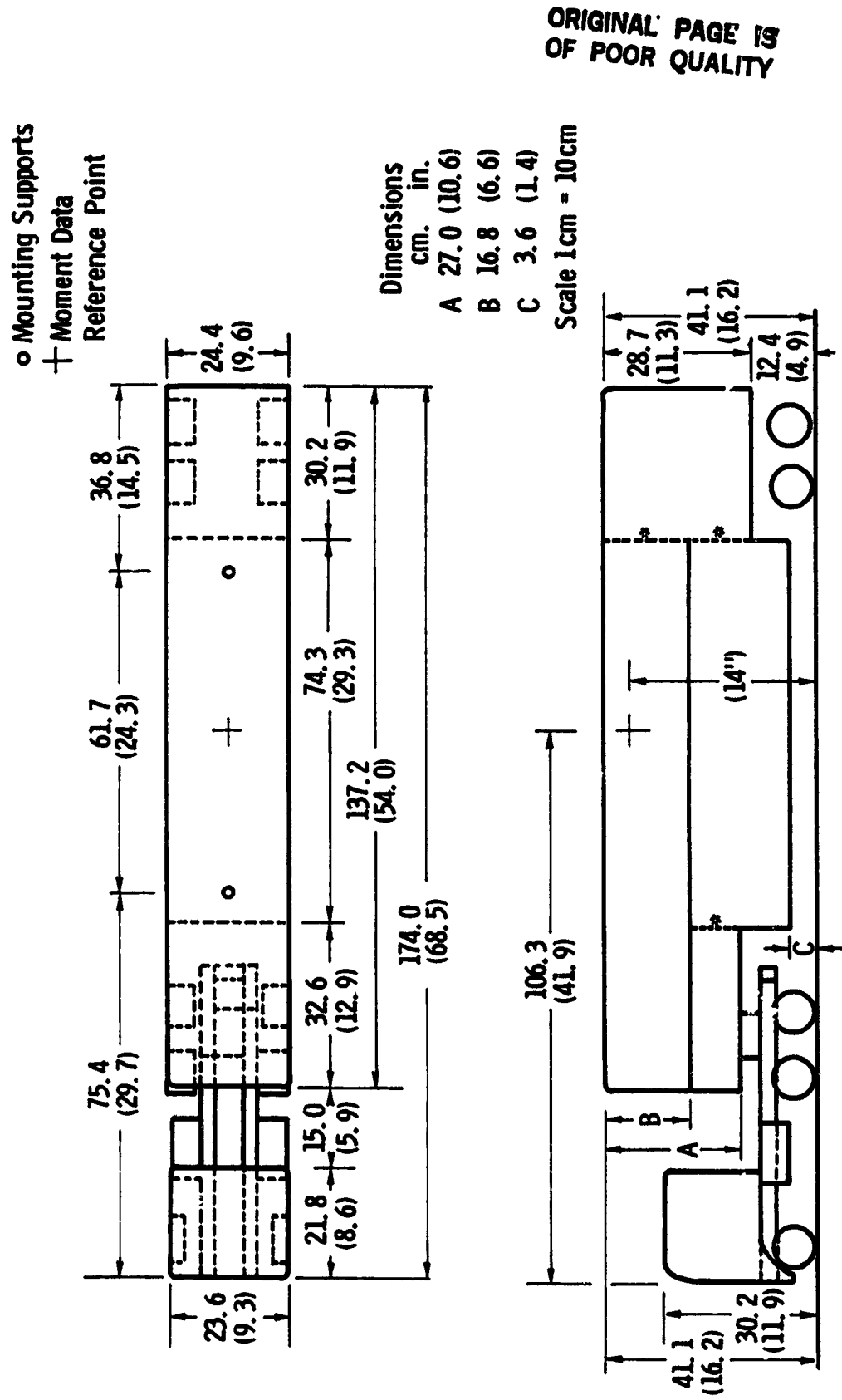
1. Stevens, D. G. and Hahn, G. L., "Air Transport of Livestock - Environmental Needs," ASAE Paper No. 77-4523, American Society of Agriculture Engineers Winter Meeting, Chicago, Ill., December 13-16, 1977.
2. Grandin, Temple, "The Effect of Stress on Livestock and Meat Quality Prior to and During Slaughter," INTP STUD ANIM PROB M(5) 1980.
3. Grandin, Temple, "Handling, Livestock," Agri Practice, May 1979.
4. Seubert, Terrence V., "Handling & Transport of Bob Calves & Special Fed Veal Calves," Paper, L.C.I. 66th Annual Meeting, Louisville, Ky, April 13, 1982.
5. James, Paul E. "Modification of Enclosed Trailers to Transport Disease-Exposed cattle," ASAE Paper No 76-6510 and Structures and Environment Division of ASAE Vol 21, No. 3, September, 1977.
6. McGan, H. L. "Double-Decked Stock Truck Cooling and Ventilating System," United States Patent No. 2,612,027, September 30, 1952.
7. Saltzman, Edwin J., "Low-Drag Ground Vehicle Particularly Suited for Use in Safely Transporting Livestock," United States Patent No. 4,343, 506, August 10, 1982.
8. Muirhead, V. U., "An Investigation of Drag Reduction for Tractor Trailer Vehicles," NASA CR 144877, October 1978.
9. Muirhead, V. U., "An Investigation of Drag Reduction for Tractor Trailer Vehicles with Air Deflector and Boattail," NASA CR 163104, January 1981.
10. Steers, L. L., and Saltzman, E. J., "Reduced Truck Fuel Consumption through Aerodynamic Design," Journal of Energy, Vol. 1, No. 5, September-October 1977.
11. Montoya, L. C., Steers, L. L. and Saltzman, E. J., "Aerodynamic Drag Reduction Tests on a Full-Scale Tractor-Trailer Combination and Representation Box-Shaped Ground Vehicles," Society of Automotive Engineers, SAE Paper 750703, August 1975.
12. Montoya, L. C., and Steers, L. L., "Aerodynamic Drag Reduction Tests on a Full-Scale Tractor Trailer Combination with Several Add-on Devices," NASA TMX-56028, December 1974.
13. Muirhead, V. U., and Saltzman, E. J., "Reduction of Aerodynamic Drag and Fuel Consumption for Tractor Trailer Vehicles," AIAA paper 79-4153, Journal of Energy, Vol. 3, No. 5, September-October 1979, p. 279.
14. Mossman, Emmet A. and Randall, Lauros M., "An Experimental Investigation of the Design Variables for NACA Submerged Duct Entrances," NACA RM No. A7I30, January 1948.

6.0 FIGURES AND TABLES

**ORIGINAL PAGE IS
OF POOR QUALITY**



Figure 2.1.1 Photograph of baseline wind tunnel model,
configuration 1.



* There vertical partitions are slotted

Figure 2.1.2 Baseline wind tunnel model, configuration 1.

**ORIGINAL PAGE IS
OF POOR QUALITY**

Numbers 1 identify measurement points indicated in Table I.

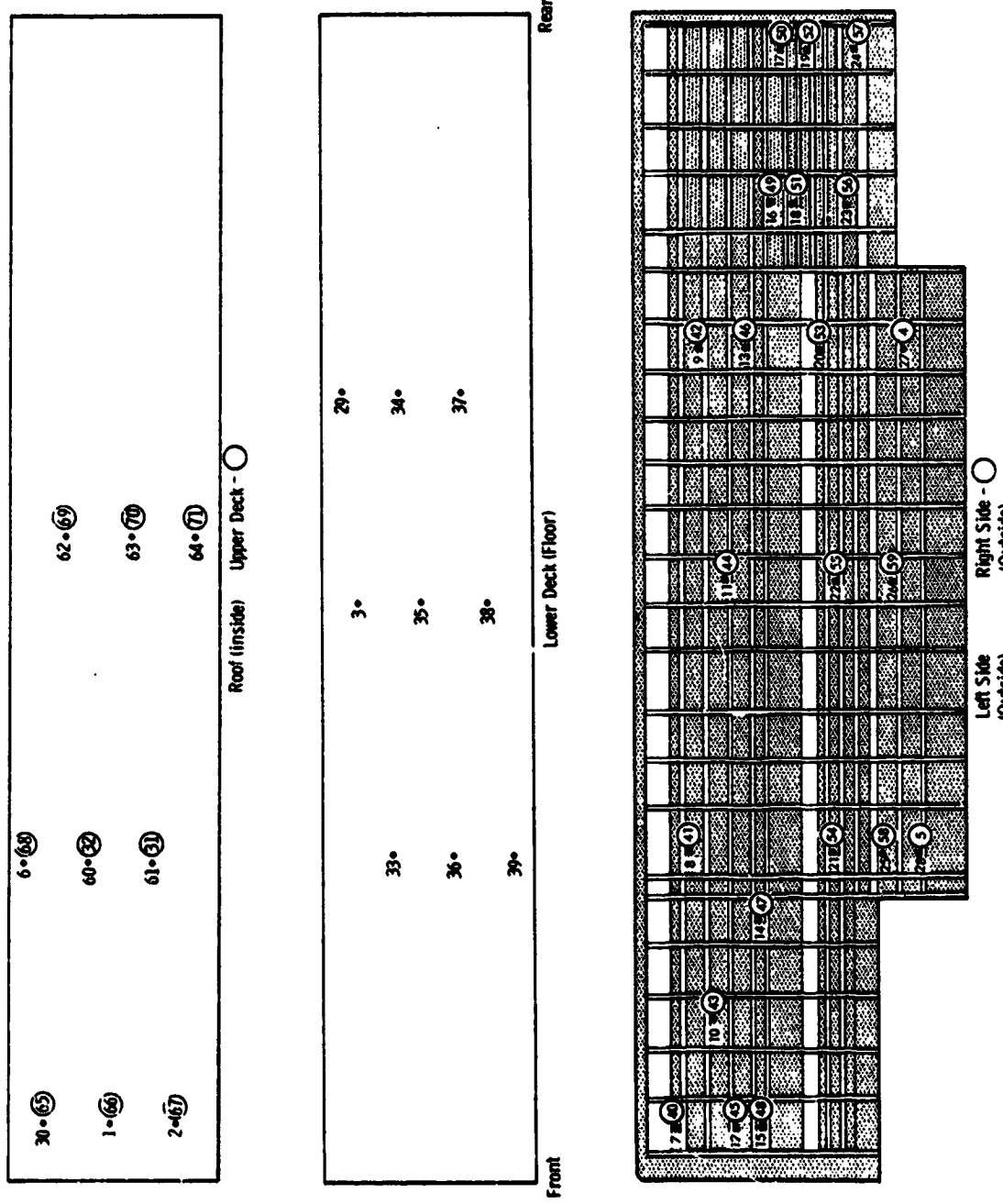
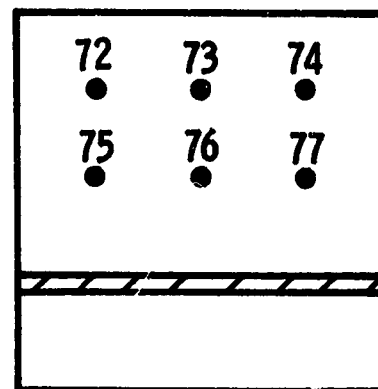


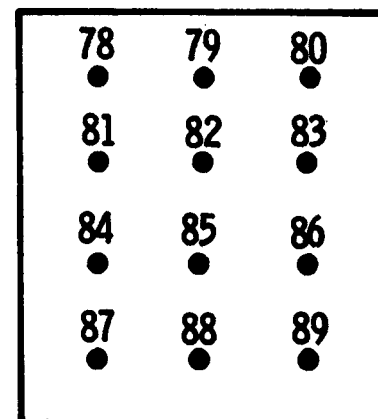
Figure 2.1.3 Pressure tap locations in baseline trailer model,
configuration 1, sides and decks.

**ORIGINAL PAGE IS
OF POOR QUALITY**

Numbers identify measurement points indicated in Table I.



**Front End (F)
Looking Forward
(Inside)**



**Back End (B)
Looking Forward
(Inside)**

**Figure 2.1.4 Pressure tap locations in baseline trailer model,
configuration 1, front and rear.**

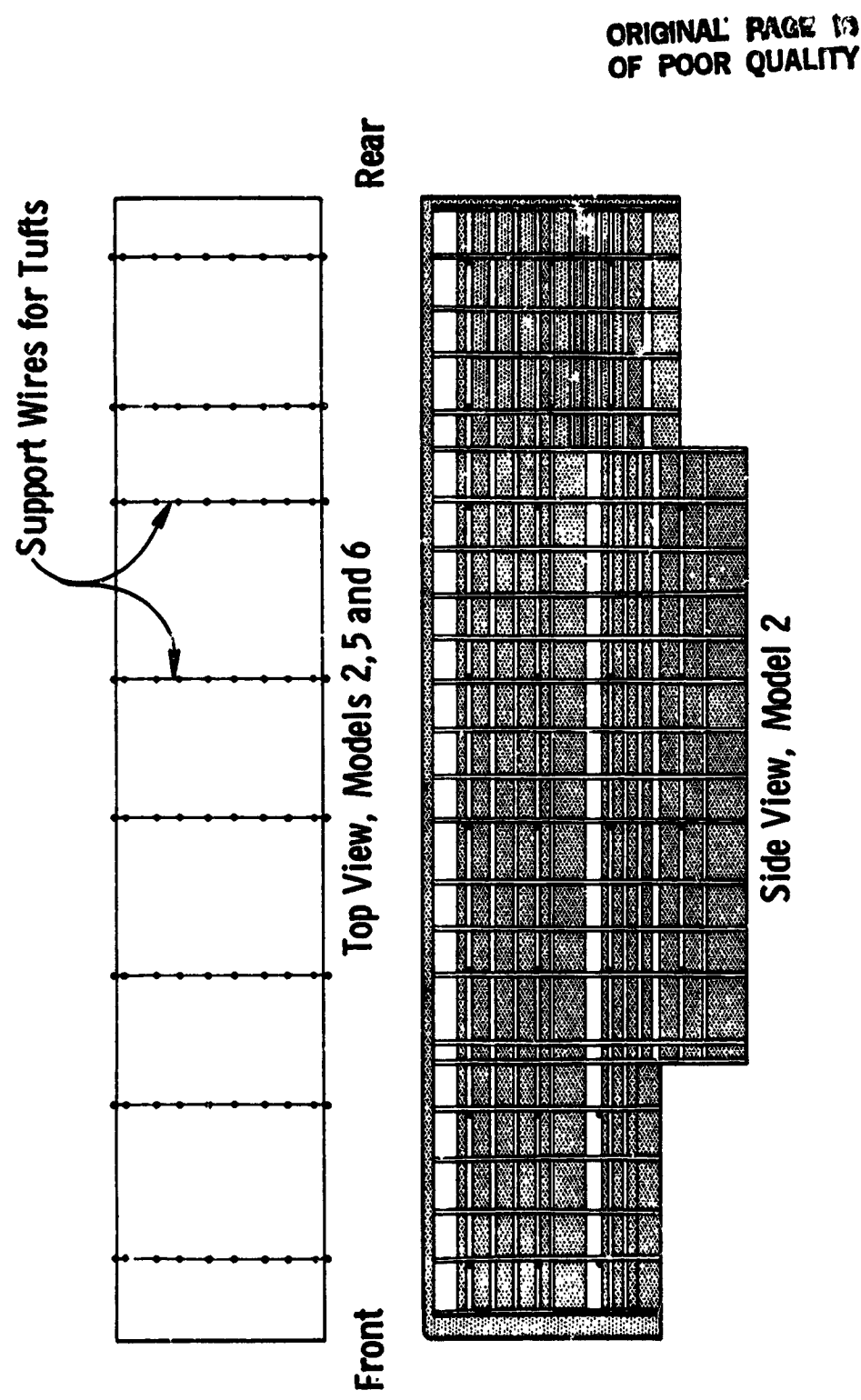


Figure 2.1.5 Tuft locations in trailer models 2, 5 and 6 (total of 280 tufts).

Letters identify measurement points indicated in Table II, III and IV.
 (R, M and L in top view correspond to right, middle and left, respectively)

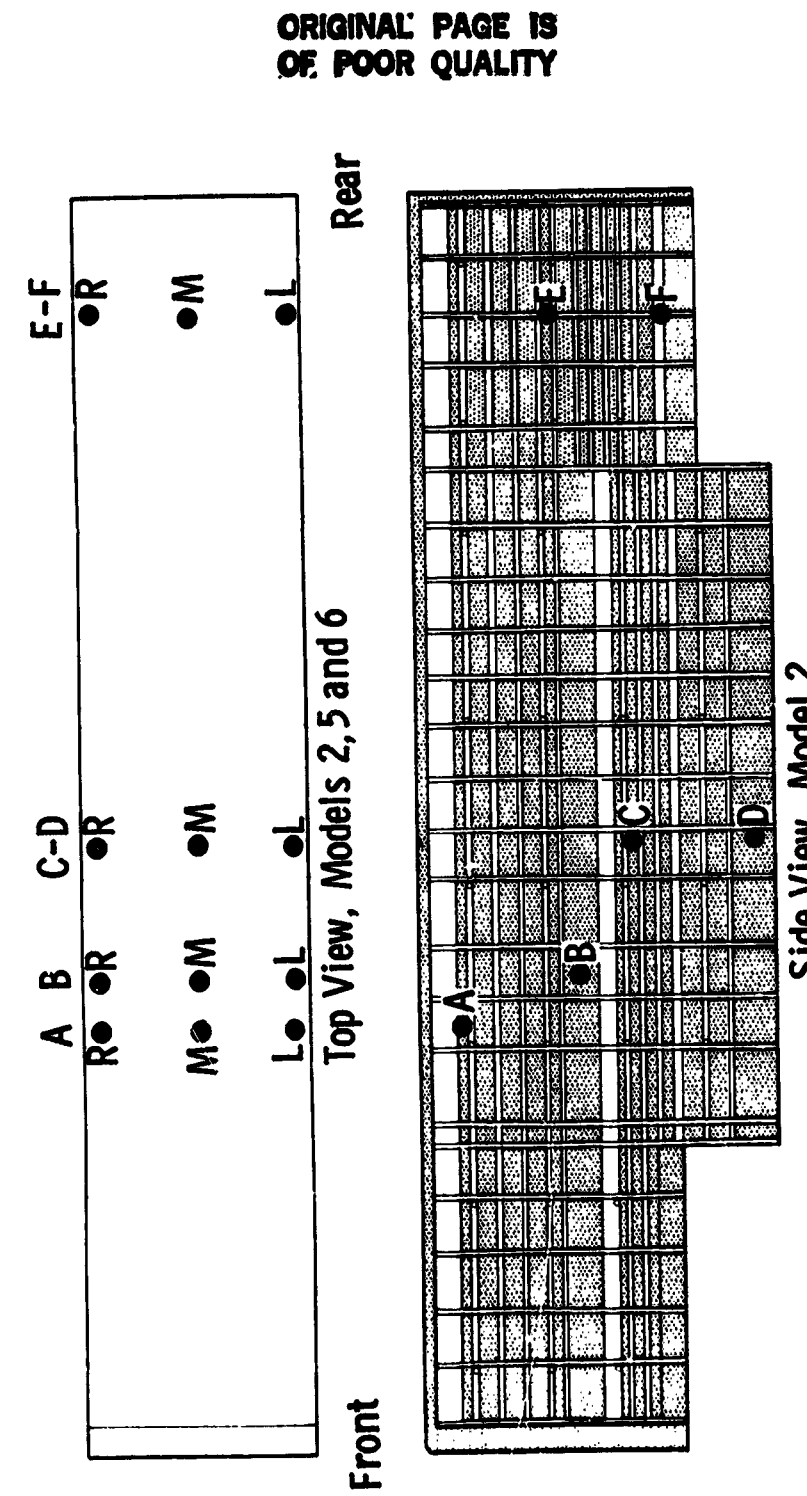


Figure 2.1.6 Airspeed measurement locations in trailer models 2, 5 and 6.

ORIGINAL PAGE IS
OF POOR QUALITY

Letters identify measurement points indicated in Table VI, VII and VIII.

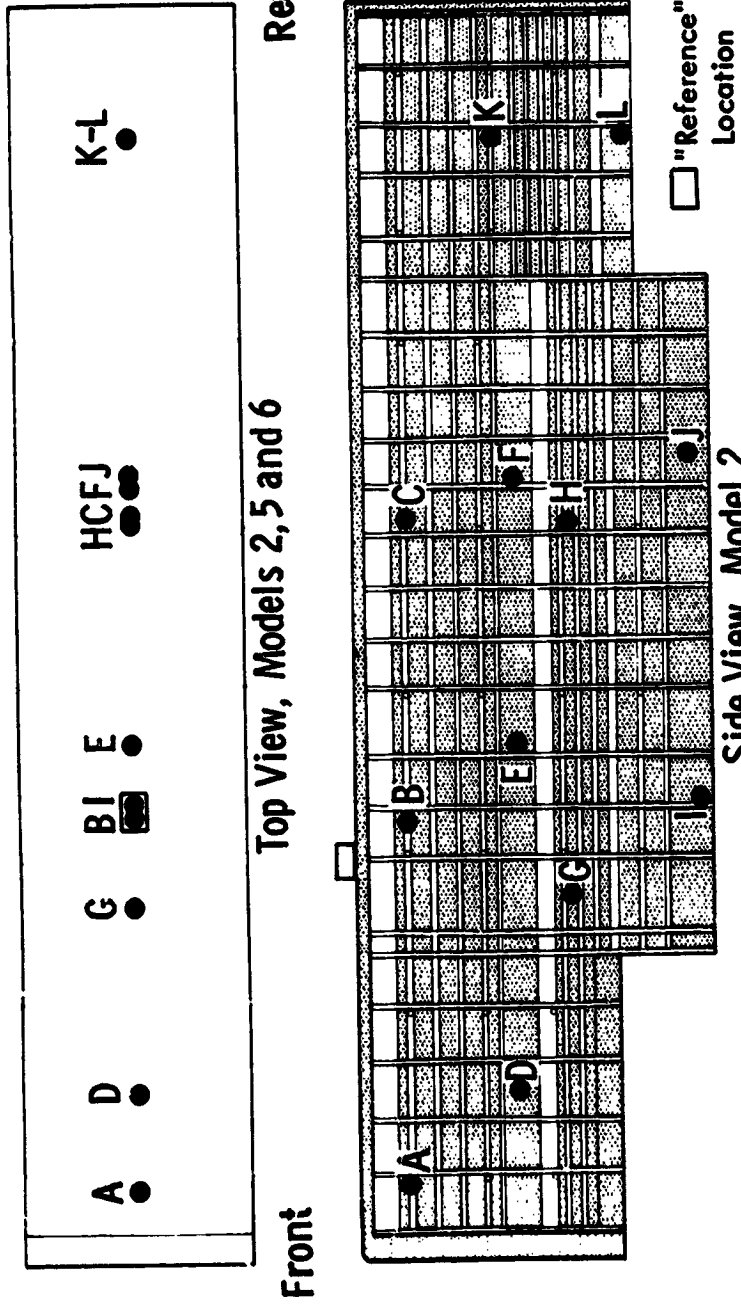


Figure 2.1.7 Ice cube locations in trailer models 2, 5 and 6 for ice cube melting tests.

**ORIGINAL PAGE IS
OF POOR QUALITY**



Figure 2.1.8 Side view of streamline wind tunnel model.

**ORIGINAL PAGE IS
OF POOR QUALITY**

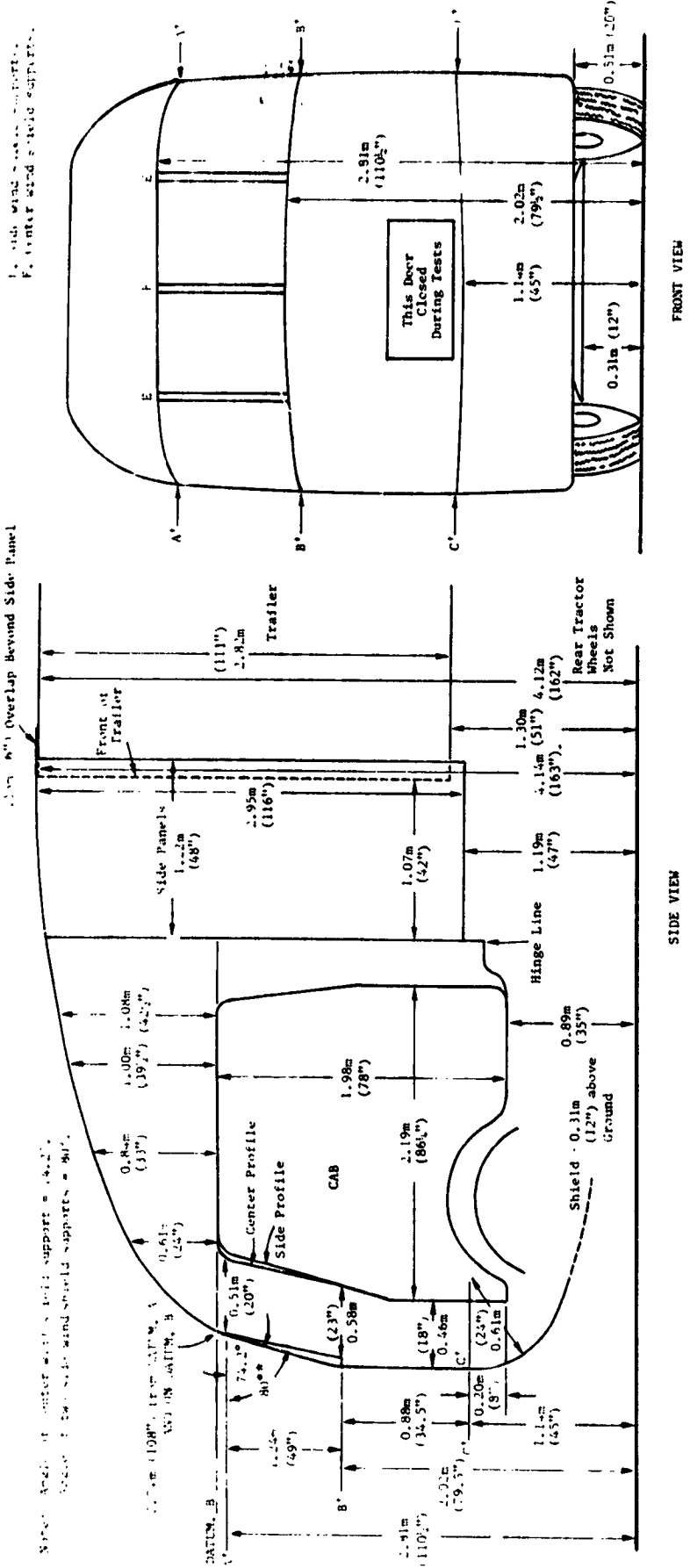


Figure 2.1.9 Forward streamlining, full scale, as in reference 8, 10 and 13.

ORIGINAL PAGE IS
OF POOR QUALITY



Figure 2.1.10 Photograph of forward streamlining and ram air inlet on configuration 5.

**ORIGINAL PAGE IS
OF POOR QUALITY**

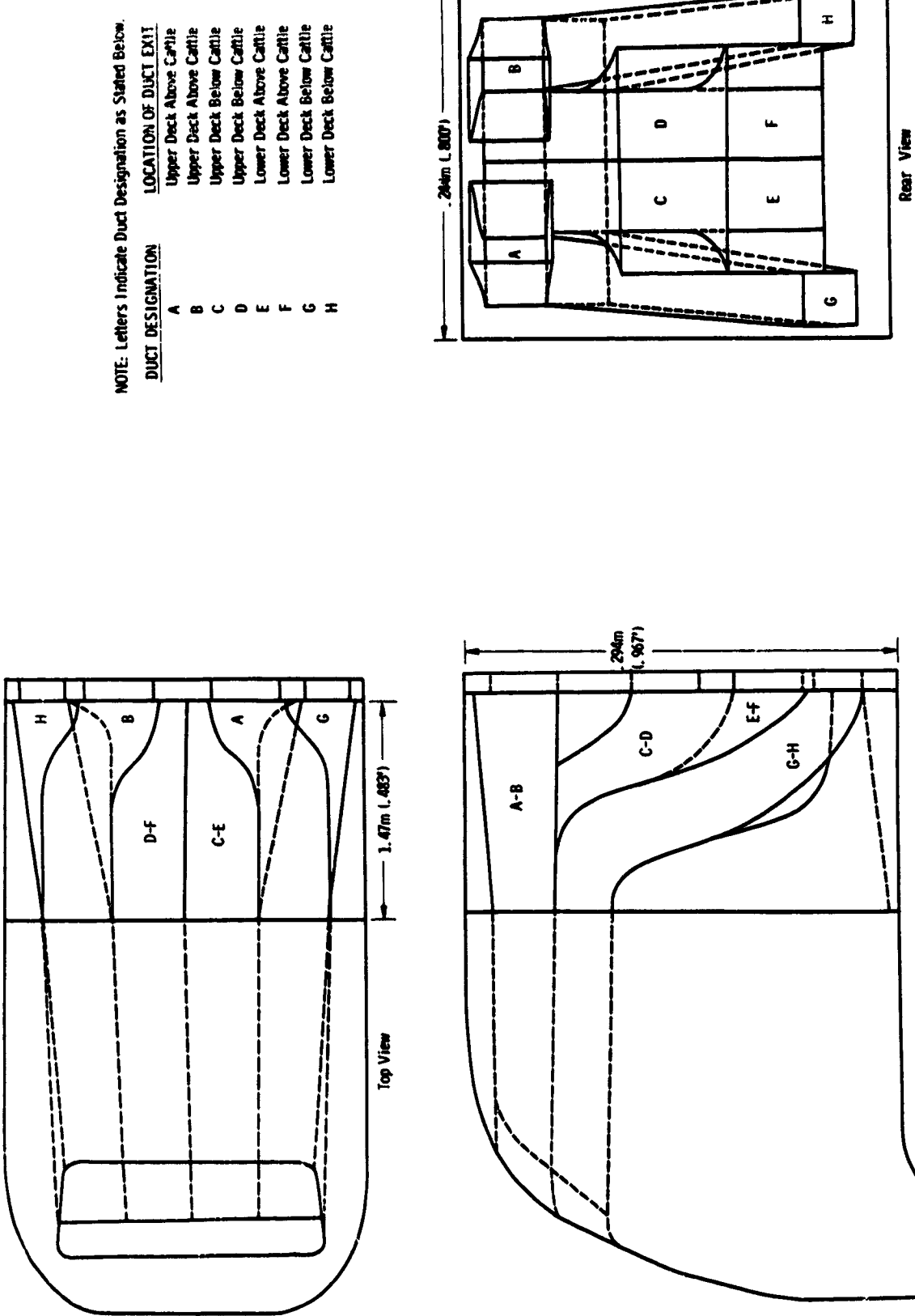


Figure 2.1.11 Ram air inlet and ducting design applied to configuration 5.

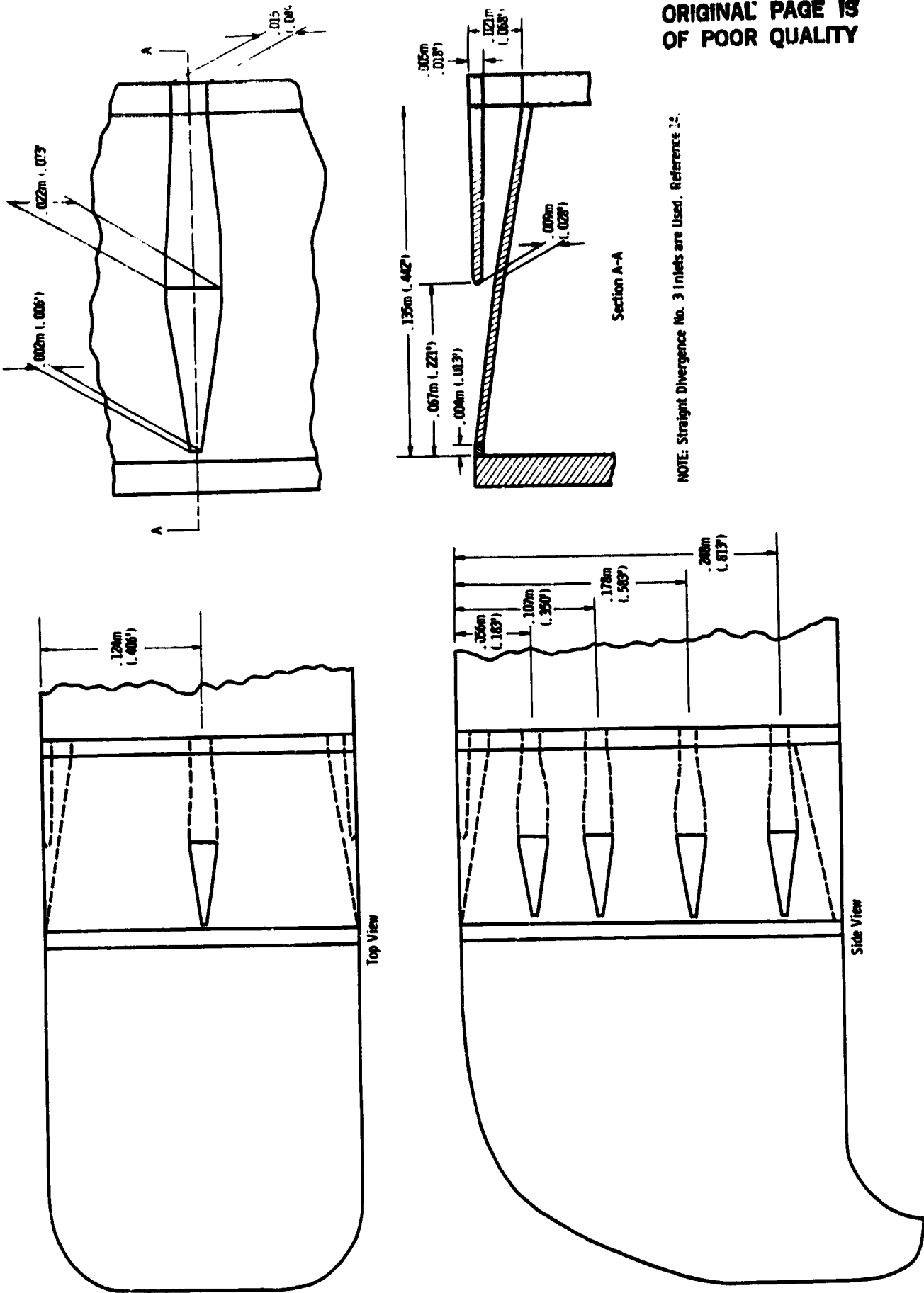


Figure 2.1.12 NACA submerged inlet and ducting design applied to configuration 6.

ORIGINAL PAGE IS
OF POOR QUALITY

Location	A cm (in)	B cm (in)	C cm (in)	# of Model Cattle
Upper Deck	91.4 (36.0)	22.9 (9.0)	14.0 (5.5)	13
Lower Deck	59.7 (23.5)	22.9 (9.0)	14.0 (5.5)	8
Rear Deck	22.9 (9.0)	22.9 (9.0)	14.0 (5.5)	3

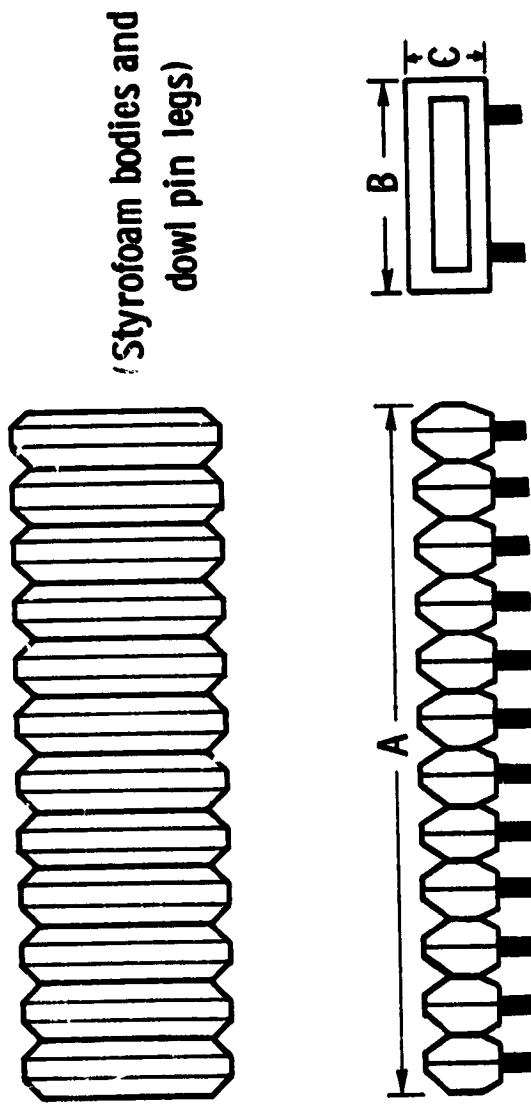
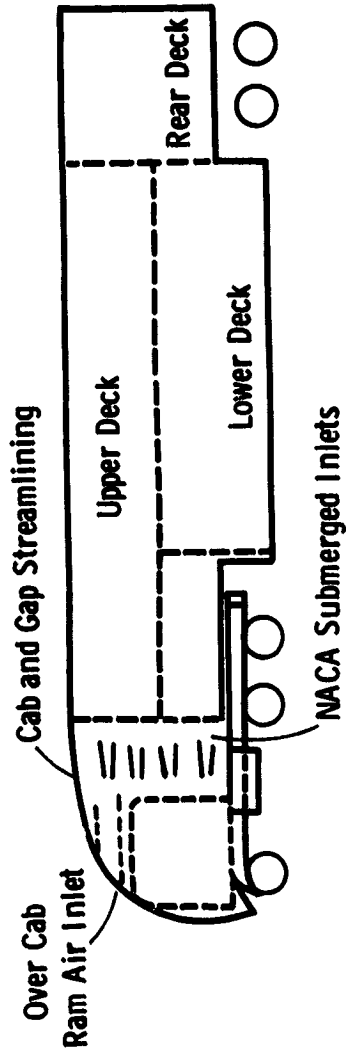


Figure 2.1.13 Cattle simulation design.

ORIGINAL PAGE IS
OF POOR QUALITY



NACA Submerged Inlets

Configuration Number	Figure	Tractor Trailer	Cattle Upper Deck	Cattle Lower Deck	Rear Deck	Cattle Sides	Cab Gap Streamlining	Over Cab Inlet	NACA Inlets	Trailer Base
1*	2.1.1 to 2.1.7	X								Solid
2*	Not Shown	X	X	X	X					Solid
3	Not Shown	X				X				Solid
4	2.1.8	X	X	X	X	X	X	X		Solid
5**	2.1.10 2.1.11	X	X	X	X	X	X	X		Ventilated
6**	2.1.12	X	X	X	X	X	X	X		Ventilated

*Configurations 1 and 2 had slotted sides for the cargo compartment, all other configurations had smooth (solid) side panels for cargo compartment.

**The ram air inlet and NACA submerged inlets were not installed simultaneously, though shown on the same drawing above for illustration purposes.

Figure 2.1.14 Model configuration chart.

ORIGINAL PAGE IS
OF POOR QUALITY

Configuration	A_s	A_{sv}	A_{sv}/A_s	A_i	A_m	A_b	A_{bv}	A_{bv}/A_b
1 & 2	4533.2 (702.6)	897.2 (139.1)	19.8% (0.0)	0.0 (0.0)	0.0 (108.5)	700.3 (0.0)	0.0 (0.0)	0.0% (0.0)
5	4533.2 (702.6)	0.0 (0.0)	0.0% (0.0)	94.7 (14.7)	114.8 (17.8)	700.3 (108.5)	98.7 (15.3)	14.1% (15.3)
6	4533.2 (702.6)	0.0 (0.0)	0.0% (0.0)	17.1 (2.6)	20.5 (3.2)	700.3 (108.5)	98.7 (15.3)	14.1% (15.3)

Upper Values of Area, cm^2

Lower Values of Area, (in^2)

Figure 2.1.15 Important physical proportions for models.

ORIGINAL PAGE IS
OF POOR QUALITY

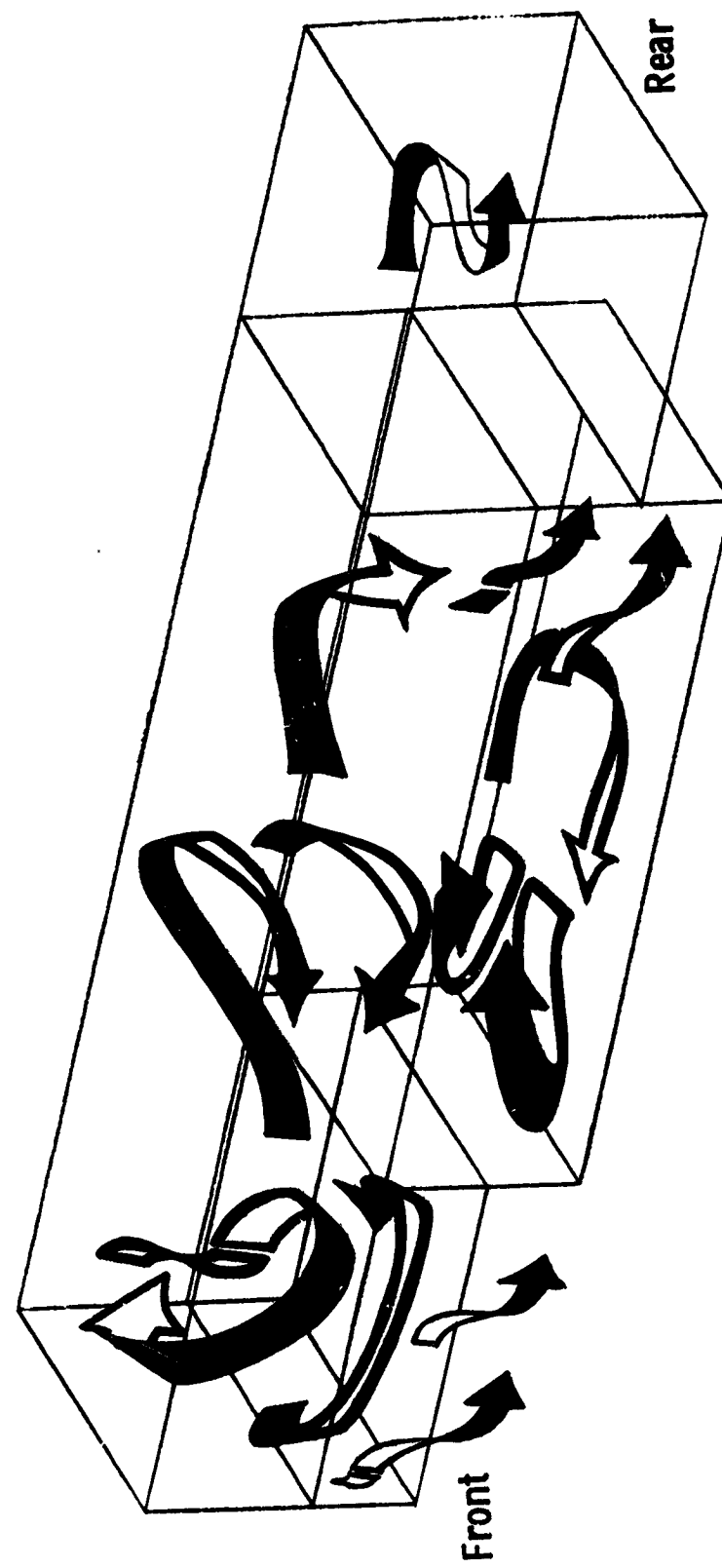


Figure 3.1.1 Air flow in trailer $\phi=0^\circ$, configuration 1,
isometric view indicating air flow direction only.

Relative Wind: $\psi = 0^\circ$

- 128 V
- 308 V

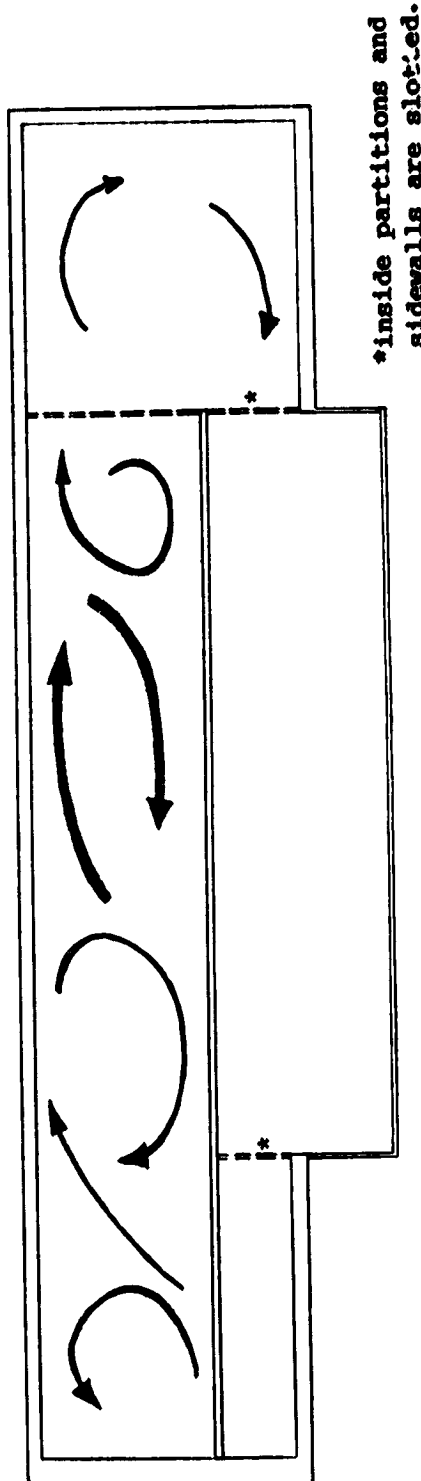
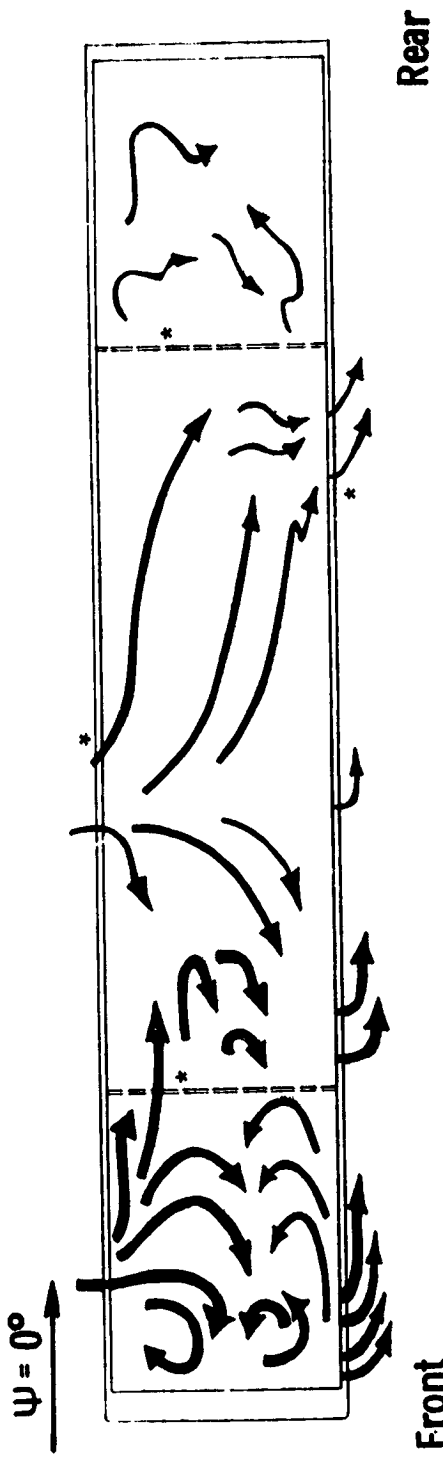


Figure 3.1.2 Air flow in trailer, $\psi = 0^\circ$, configuration 1,
upper and rear decks.

ORIGINAL PAGE IS
OF POOR QUALITY

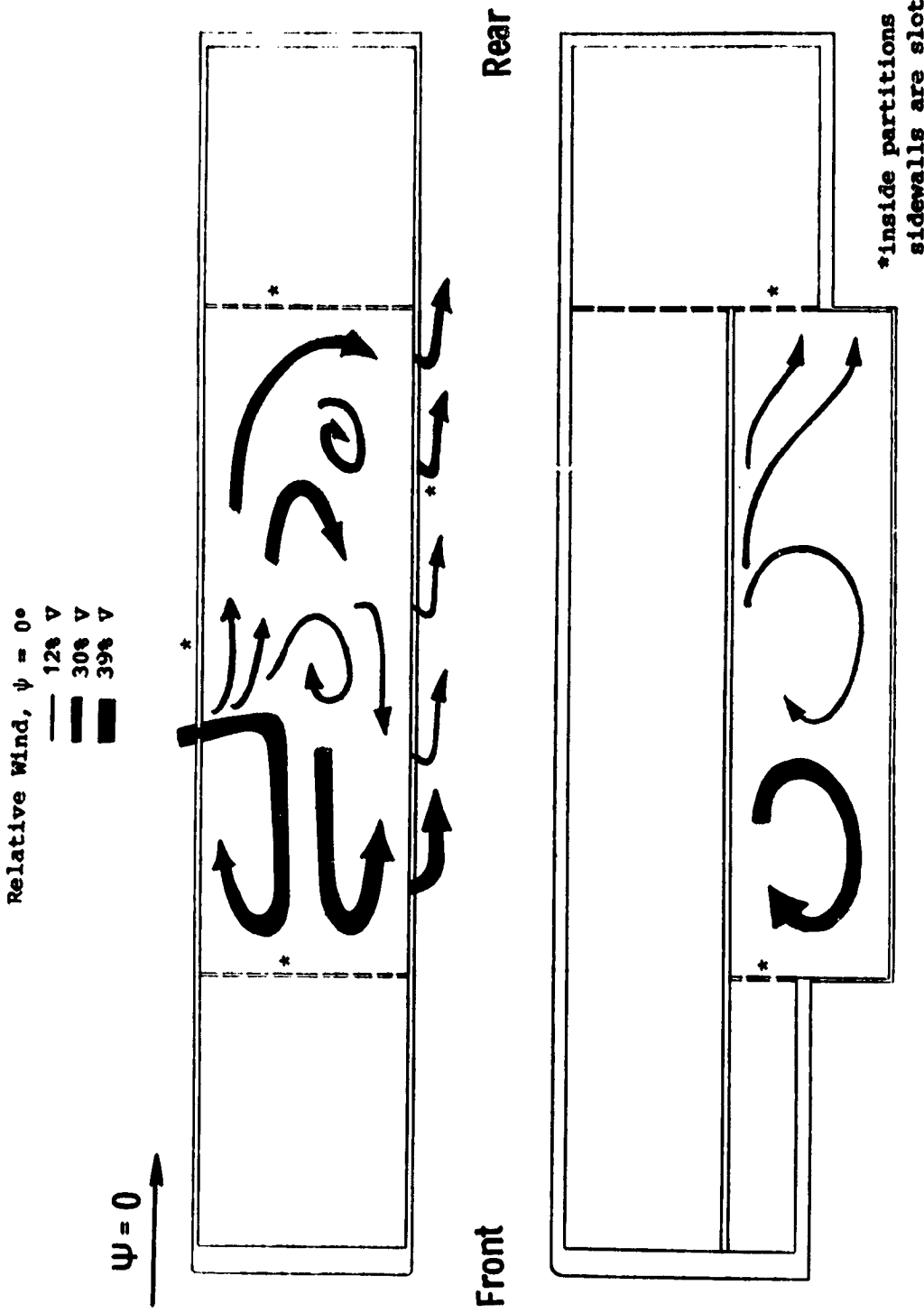


Figure 3.1.3 Air flow in trailer, $\psi = 0^\circ$ configuration 1,
lower deck.

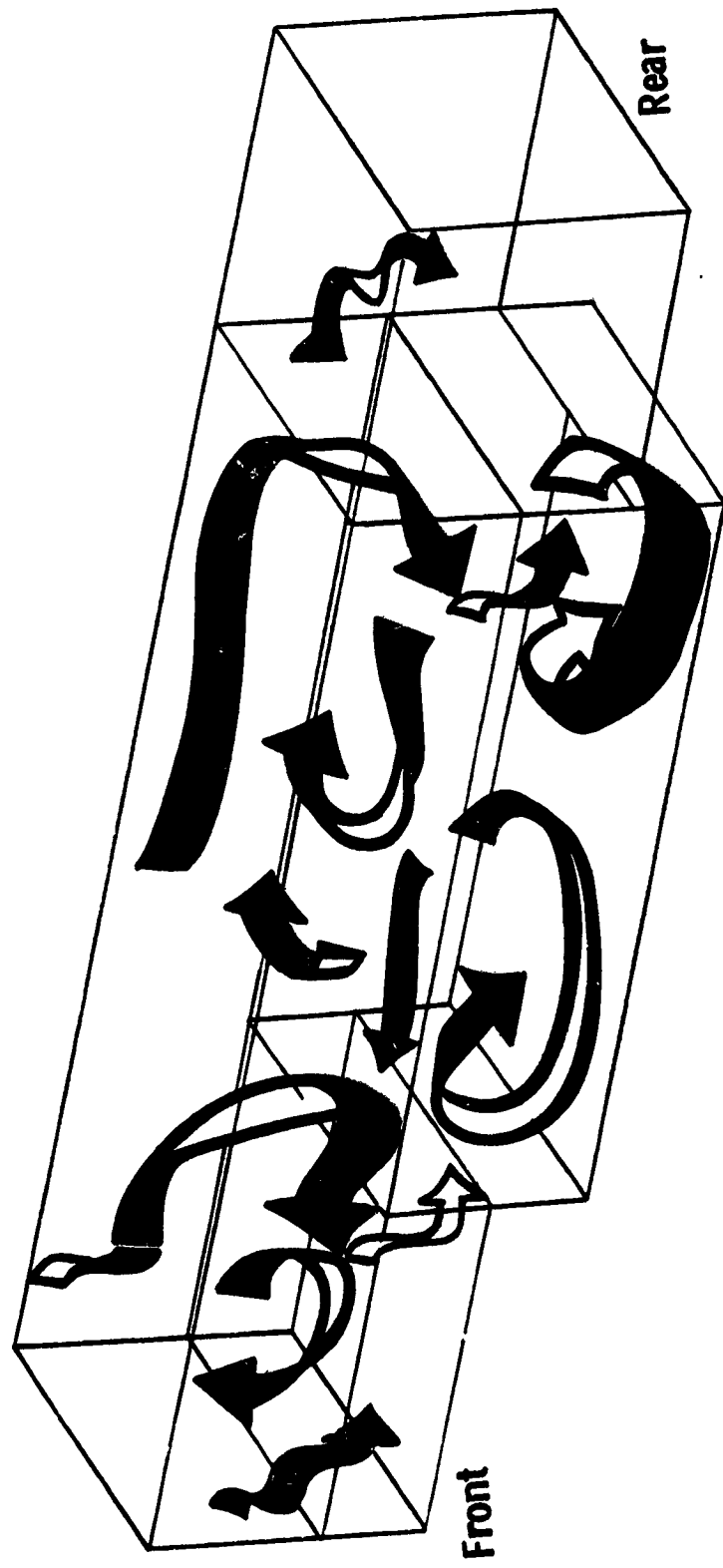


Figure 3.1.4 Air flow in trailer, $\phi = 15^\circ$ configuration 1, isometric view indicating air flow direction only.

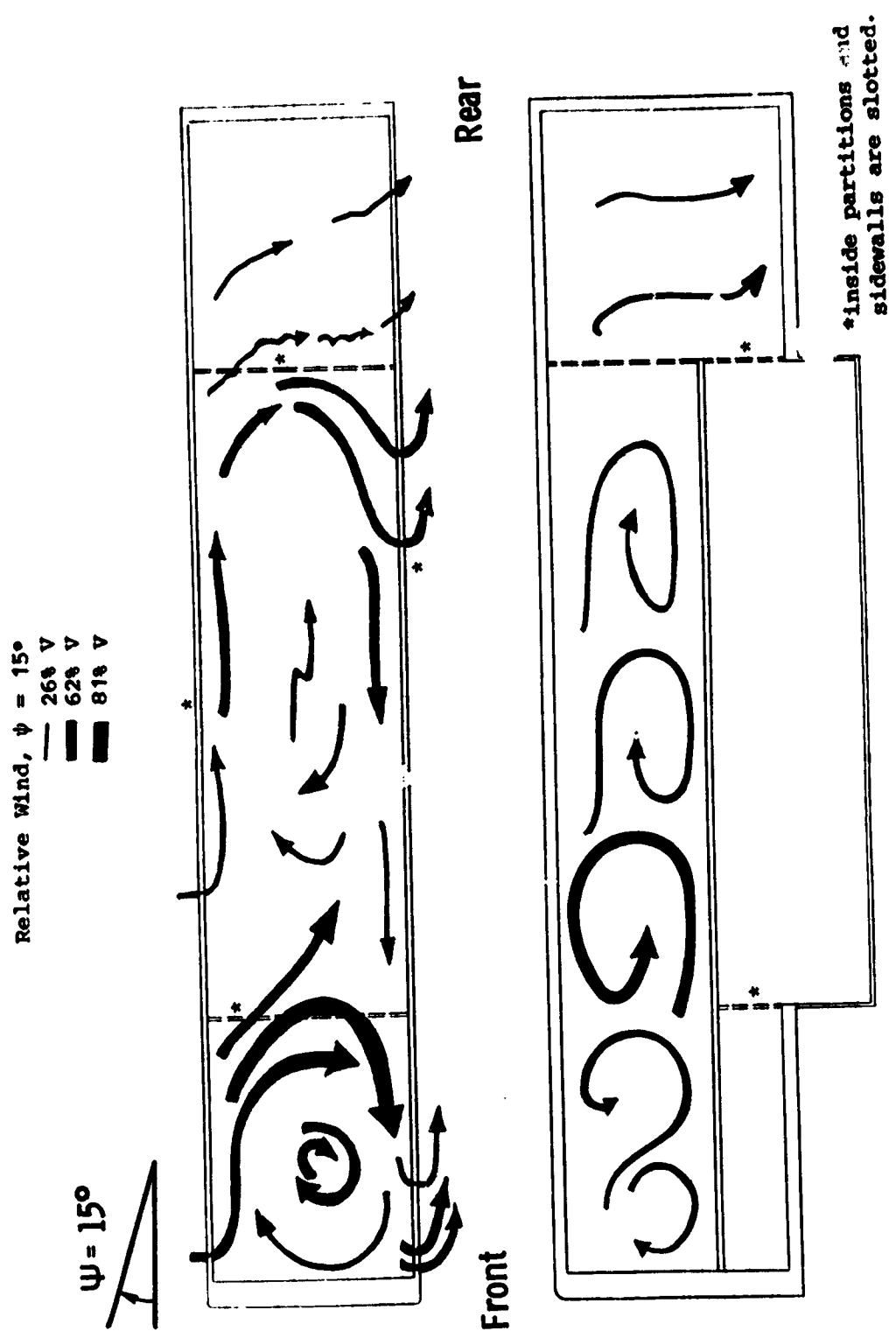


Figure 3.1.5 Air flow in trailer, $\psi = 15^\circ$, configuration 1,
upper and rear decks.

ORIGINAL PAGE IS
OF POOR QUALITY

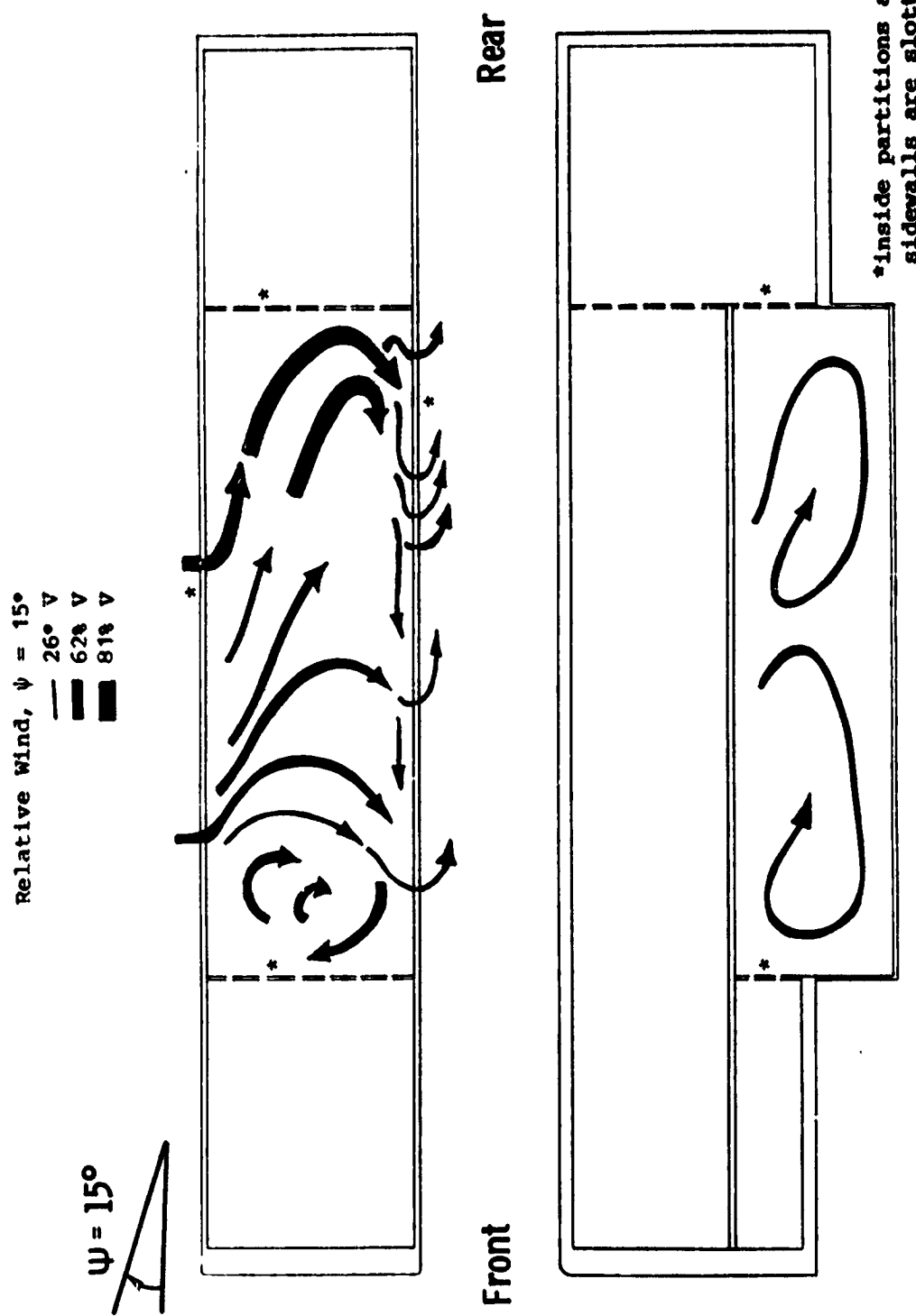
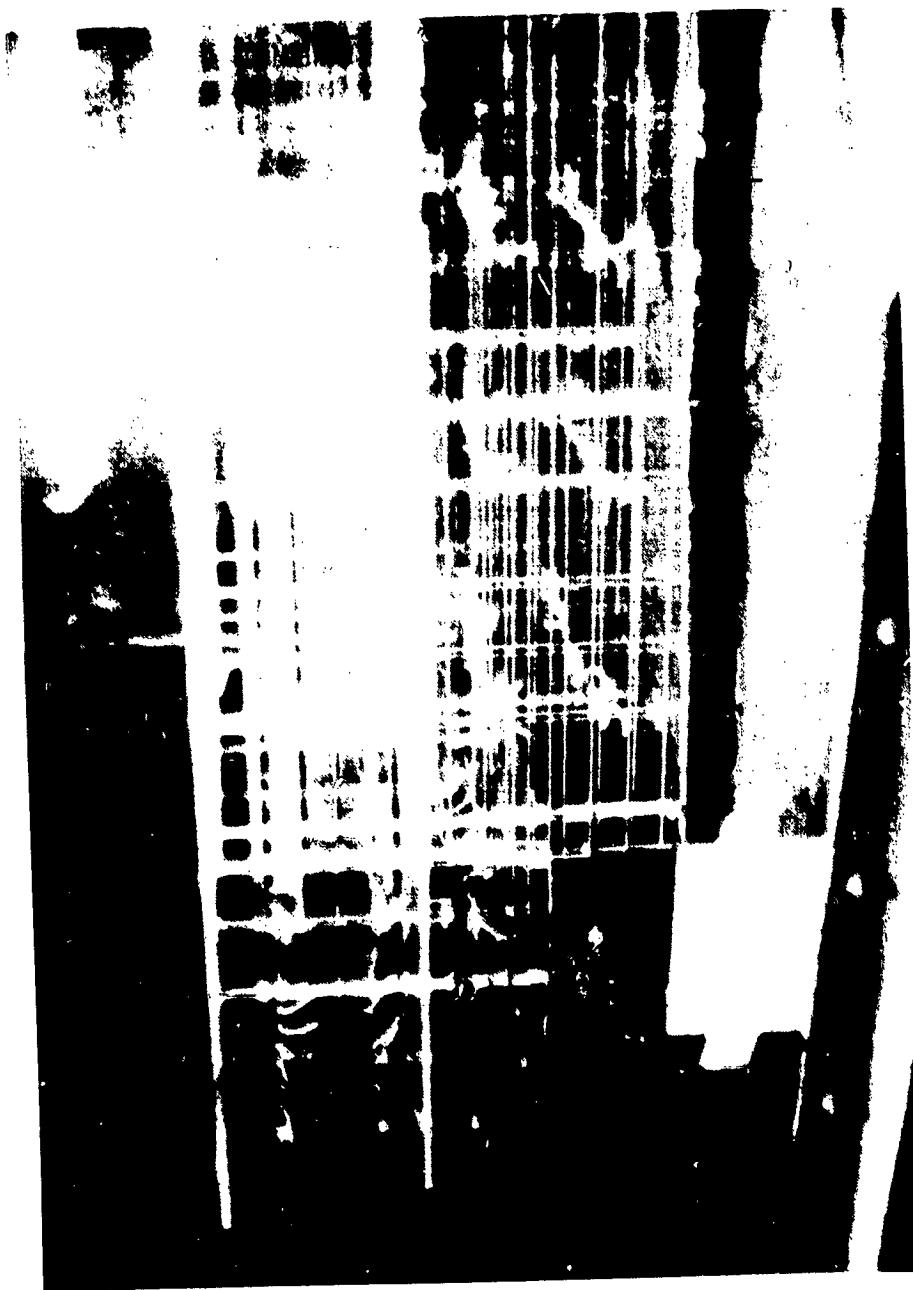


Figure 3.1.6 Air flow in trailer, $\psi 15^\circ$, configuration 1,
lower deck.

ORIGINAL PAGE IS
OF POOR QUALITY.

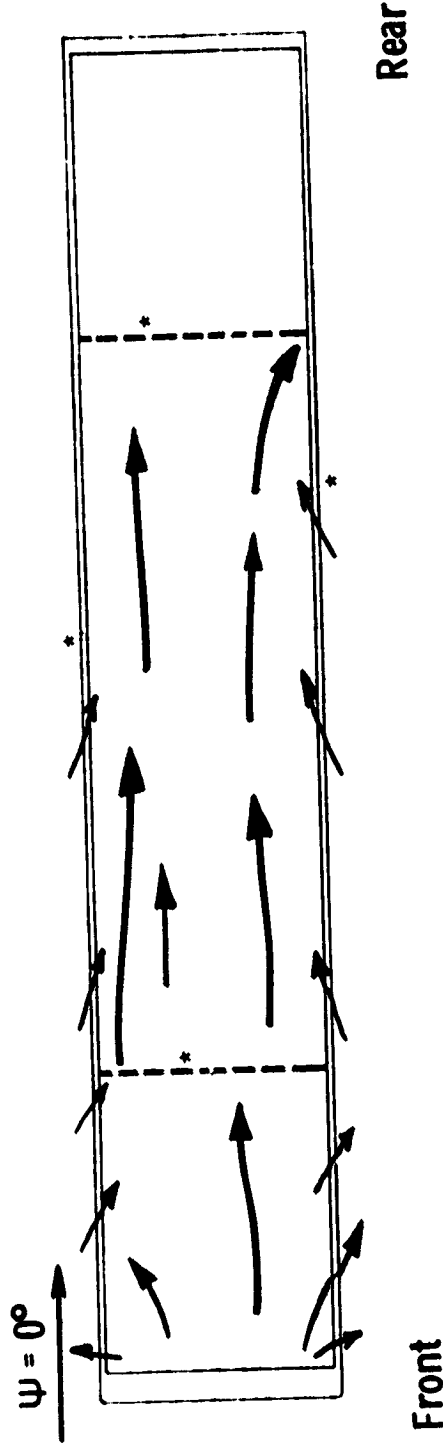
Rear



Front

Figure 3.1.7 Photograph of tufts in trailer, configuration 1, $\psi = 0^\circ$.

Relative Wind, $\psi = 0^\circ$
— $5\% v$
— $20\% v$



ORIGINAL PAGE IS
OF POOR QUALITY

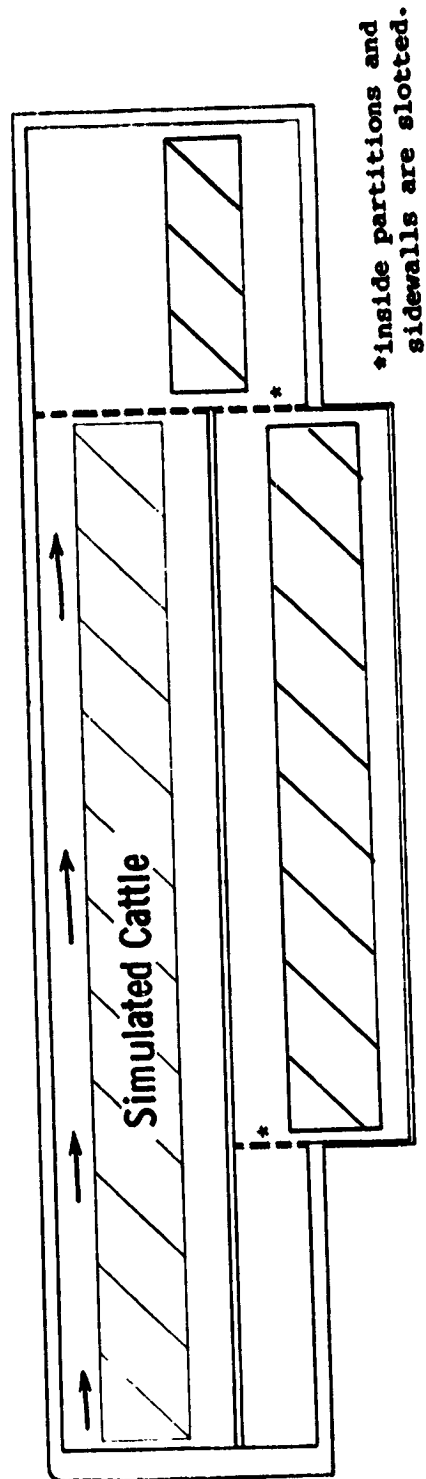


Figure 3.1.8 Air flow in trailer, $\psi = 0^\circ$, configuration 2,
upper deck above cattle.

ORIGINAL PAGE IS
OF POOR QUALITY

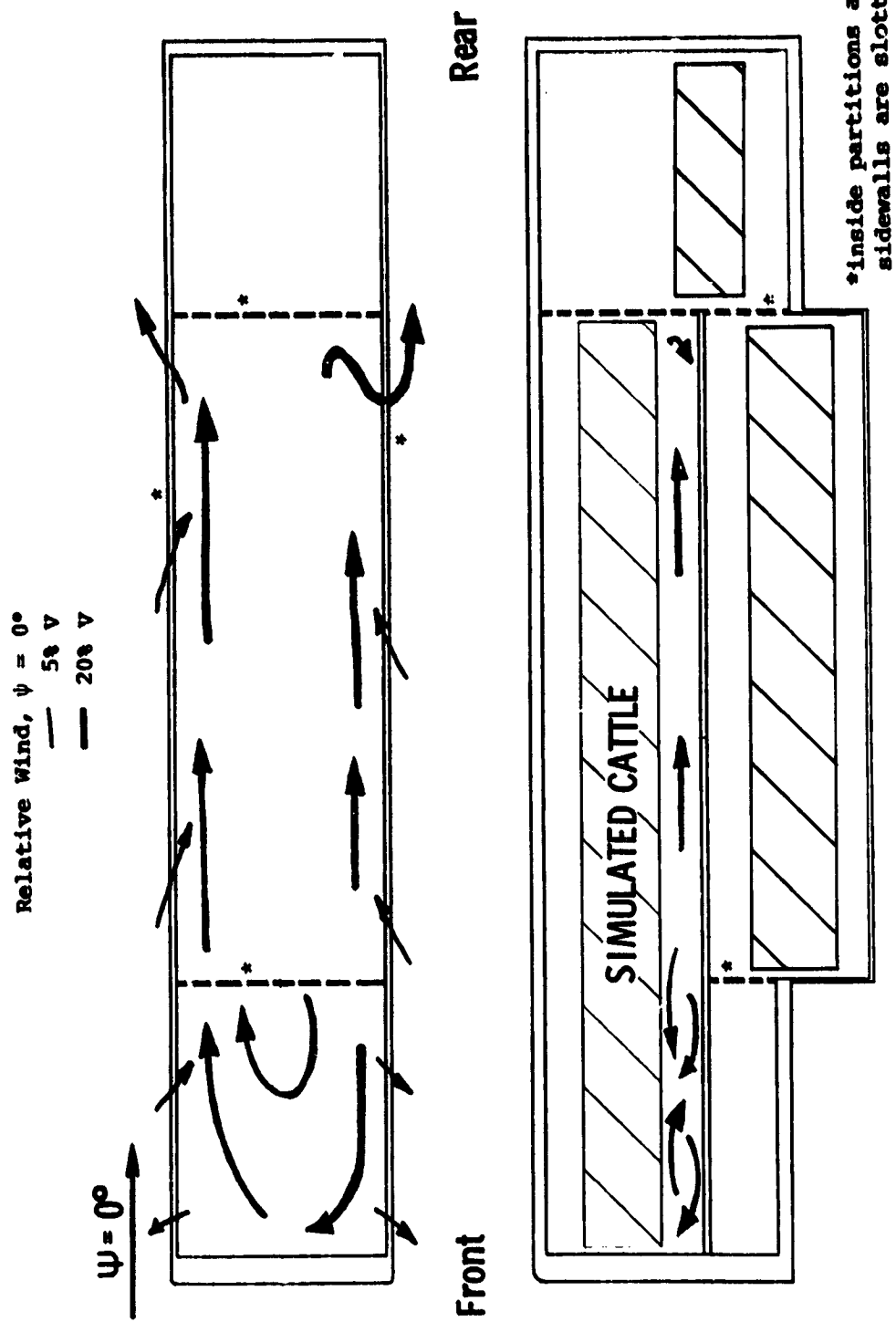


Figure 3.1.9 Air flow in trailer, $\Psi = 0^\circ$, configuration 2,
upper deck below cattle.

**ORIGINAL PAGE IS
OF POOR QUALITY**

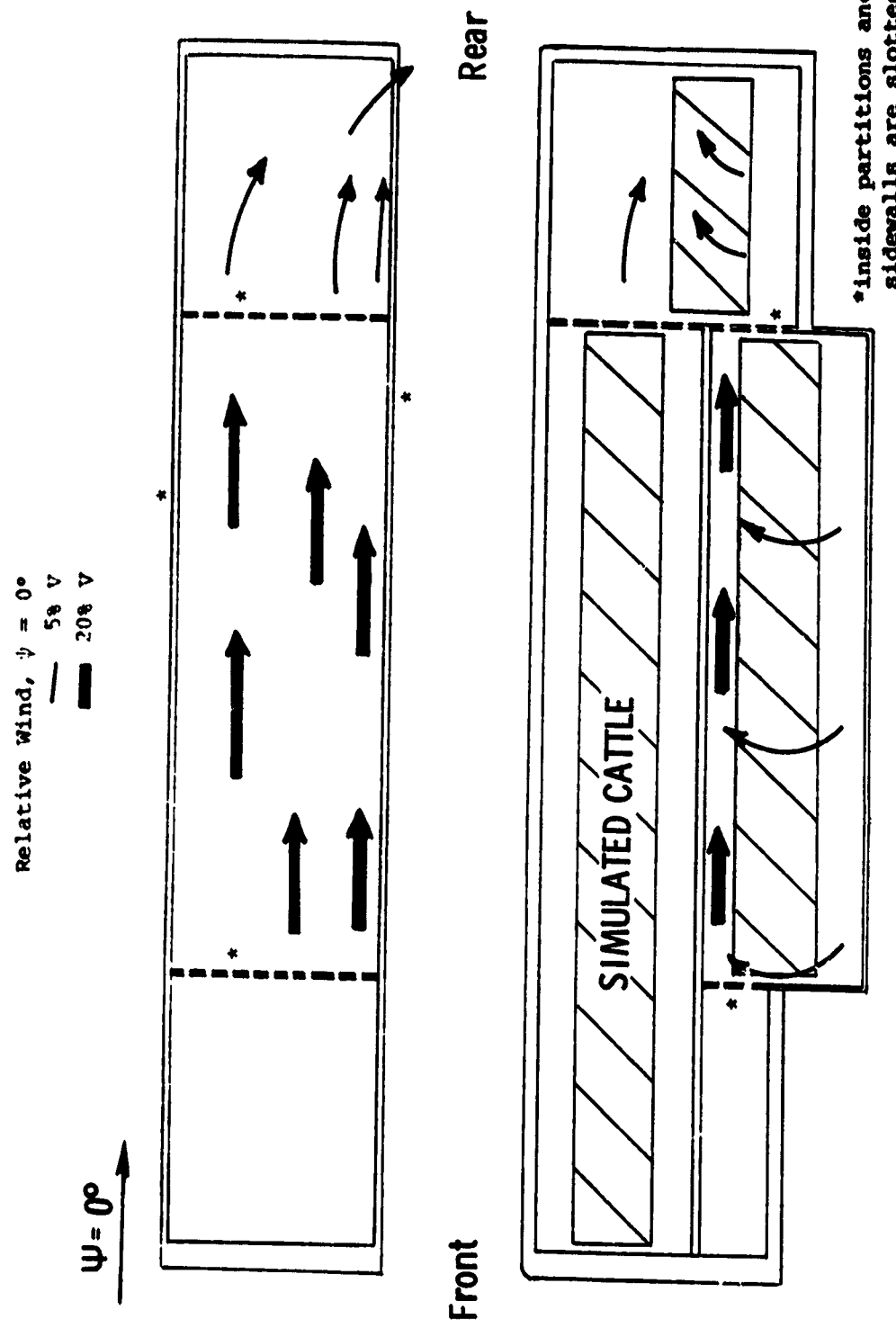


Figure 3.1.10 Air flow in trailer, $\psi = 0^\circ$, configuration 2, lower and rear decks above cattle.

ORIGINAL PAGE IS
OF POOR QUALITY.

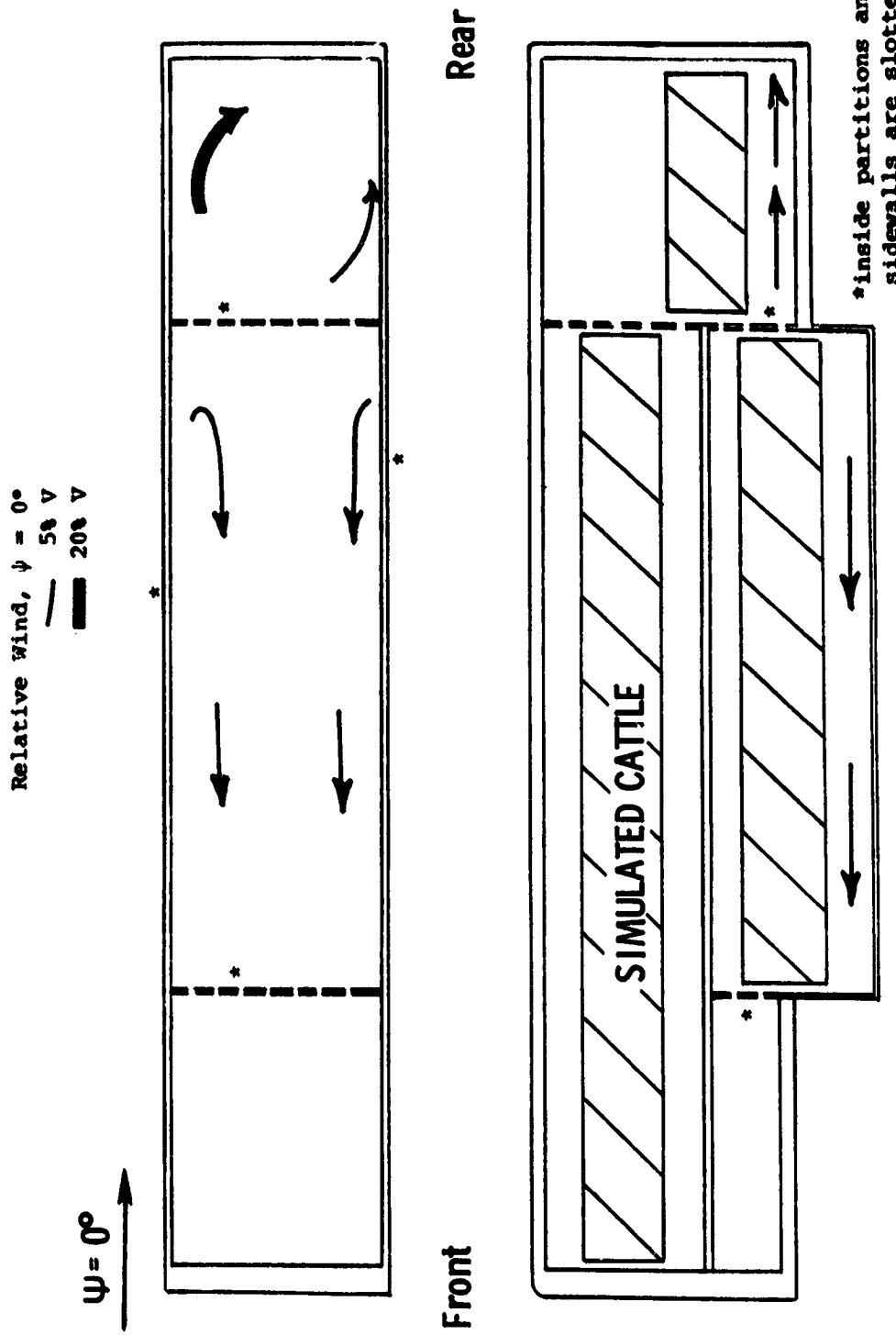


Figure 3.1.11 Air flow in trailer, $\psi = 0^\circ$, configuration 2,
lower and rear decks below cattle.

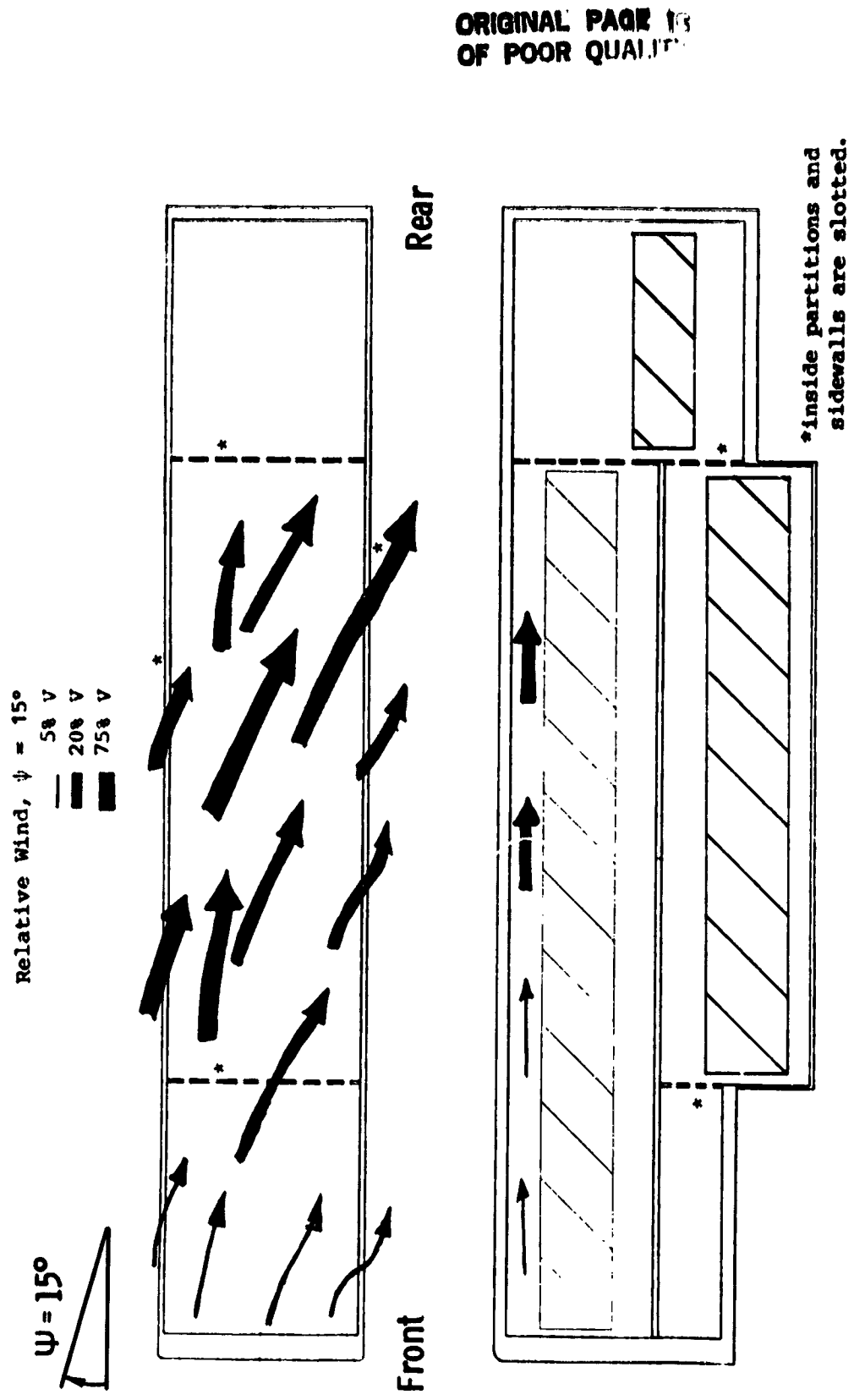


Figure 3.1.12 Air flow in trailer, $\Psi = 15^\circ$, configuration 2,
upper deck above cattle.

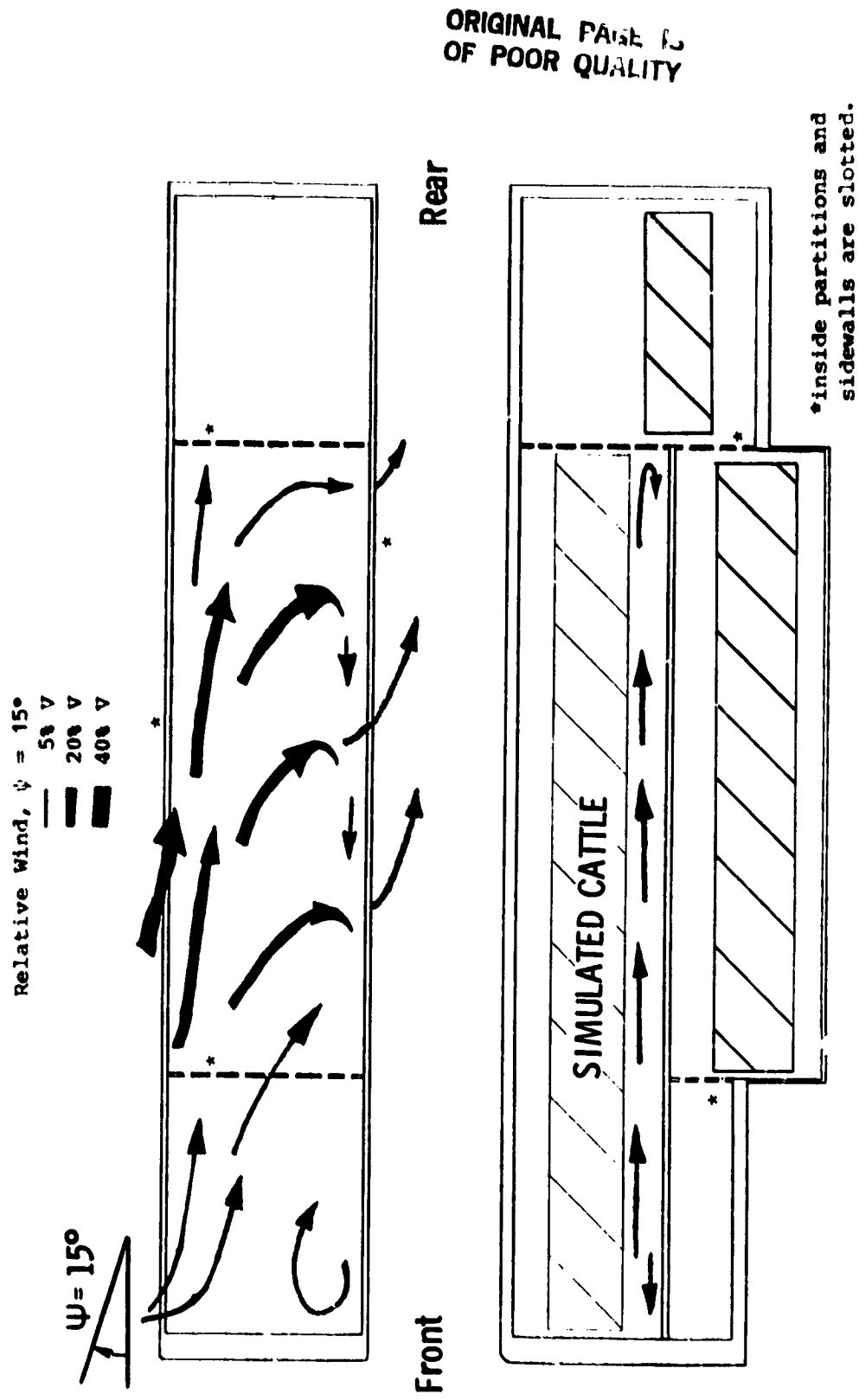
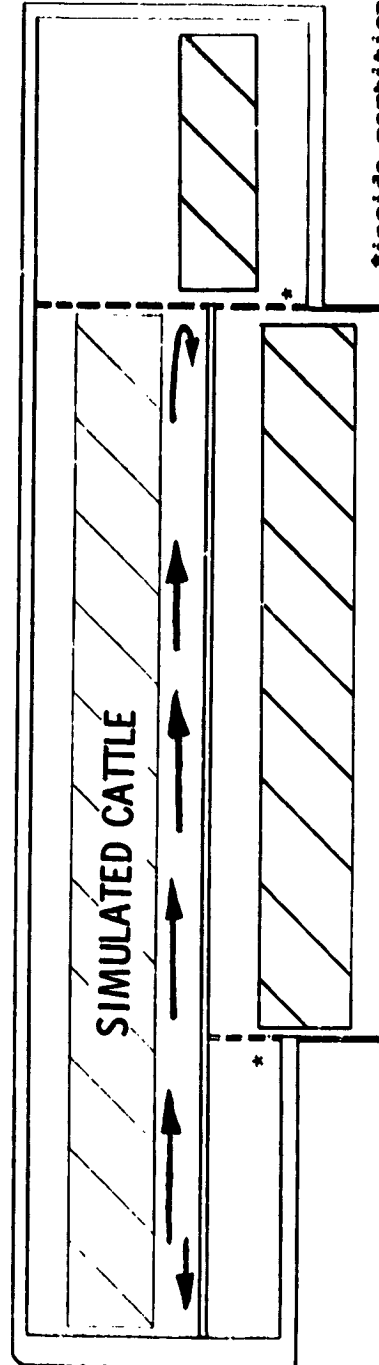
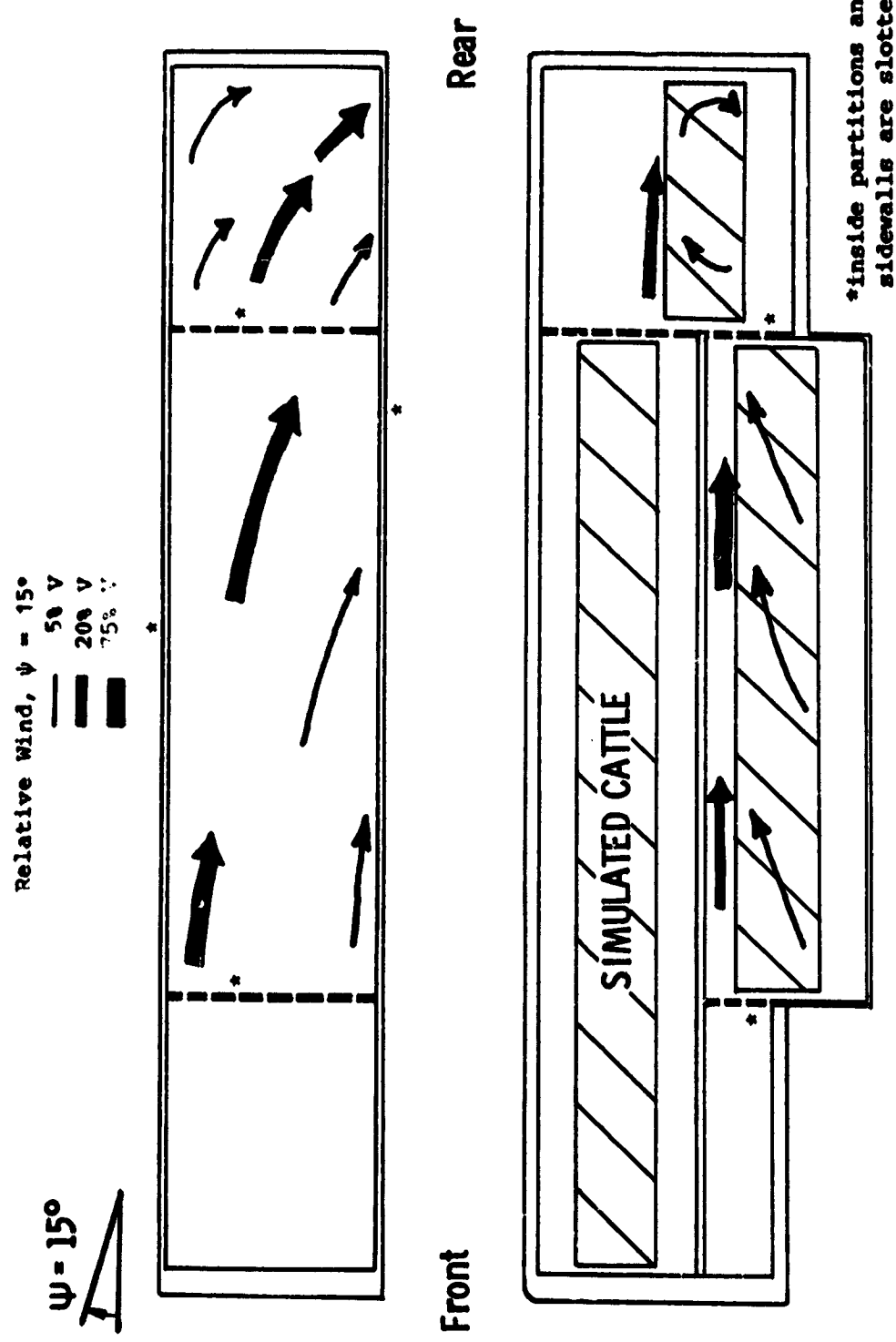


Figure 3.1.13 Air flow in trailer, $\psi = 15^\circ$, configuration 2,
upper deck below cattle.

*inside partitions and
sidewalls are slotted.



ORIGINAL PAGE IS
OF POOR QUALITY



*inside partitions and
sidewalls are slotted.

Figure 3.1.14 Air flow in trailer, $\Psi = 15^\circ$, configuration 2,
lower and rear decks above cattle.

ORIGINAL PAGE IS
OF POOR QUALITY

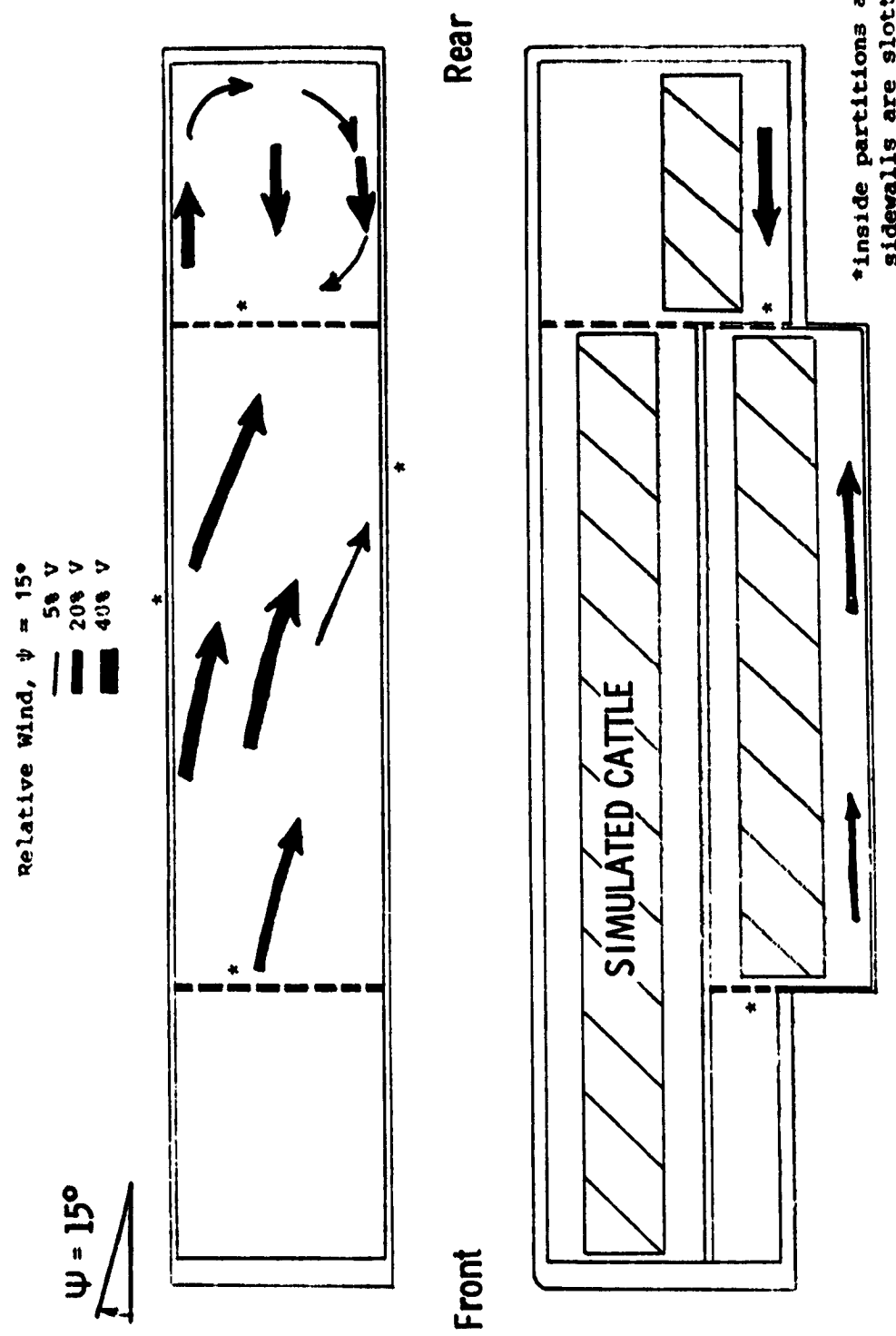
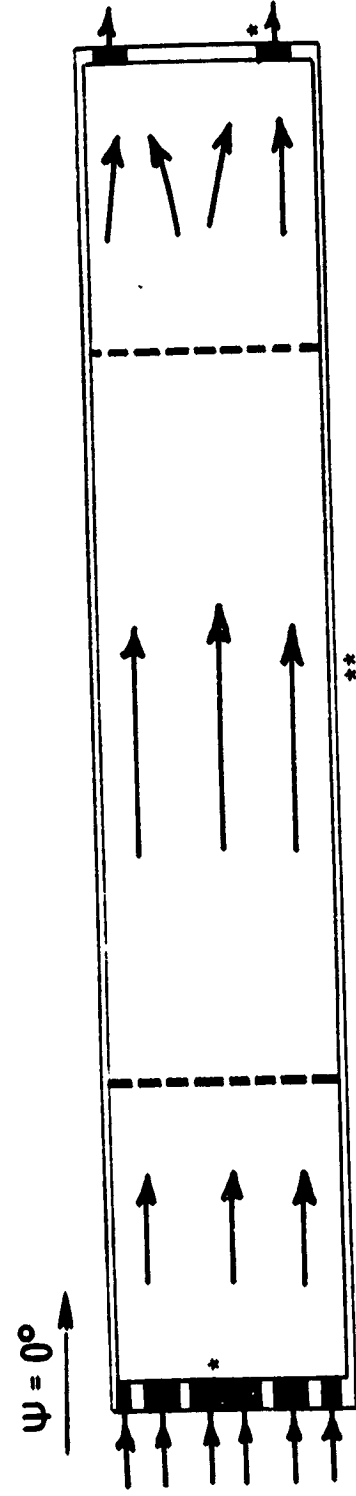


Figure 3.1.15 Air flow in trailer, $\psi = 15^\circ$, configuration 2,
lower and rear decks below cattle.

Relative Wind, $\psi = 0^\circ$
— 12a v



ORIGINAL PAGE IS
OF POOR QUALITY

Rear

Front

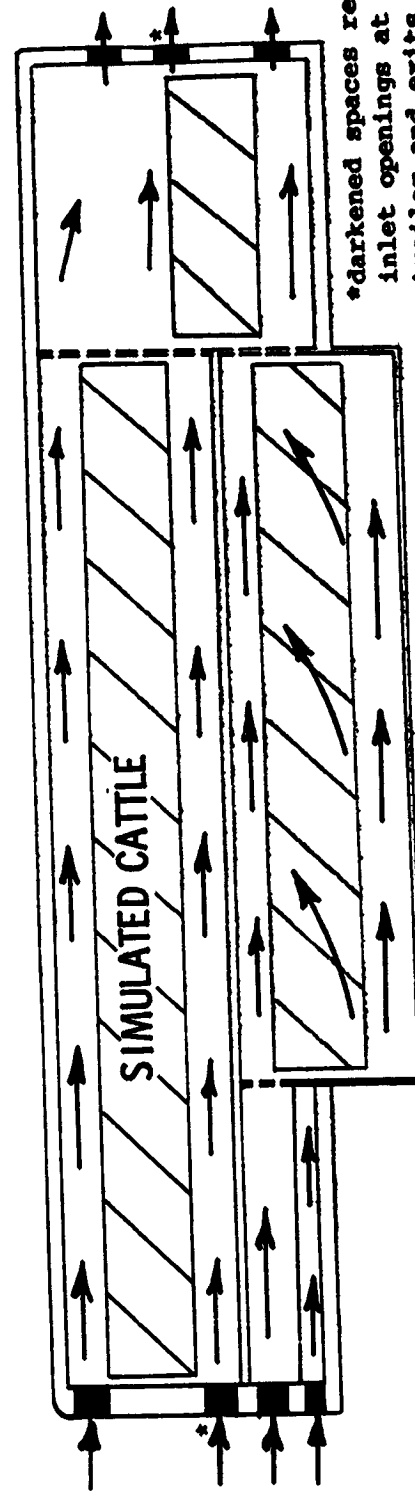


Figure 3.1.16 Air flow in trailer, $\psi = 0^\circ$, configuration 5.

ORIGINAL PAGE IS
OF POOR QUALITY

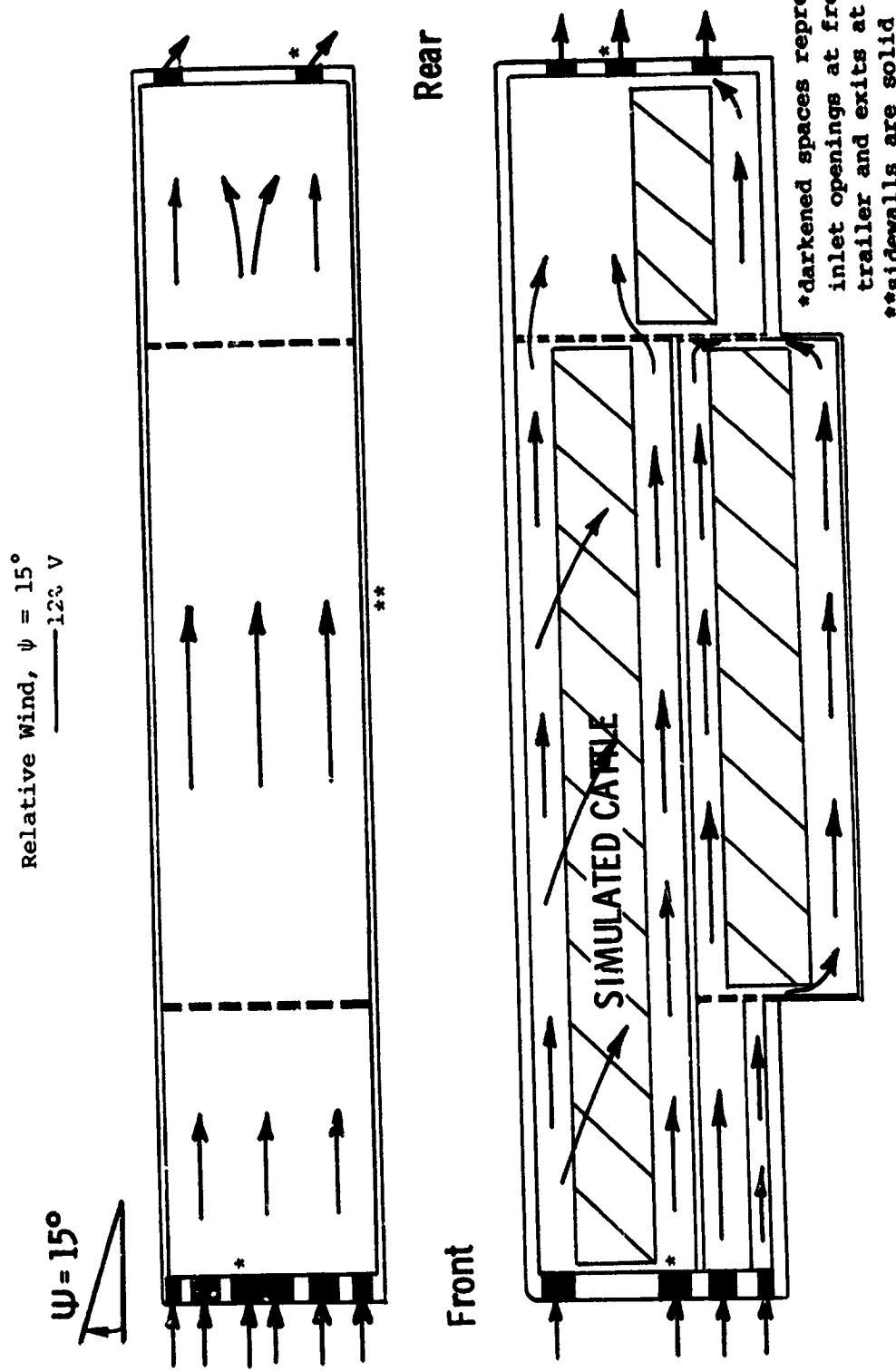


Figure 3.1.17 Air flow in trailer, $\psi = 15^\circ$, configuration 5

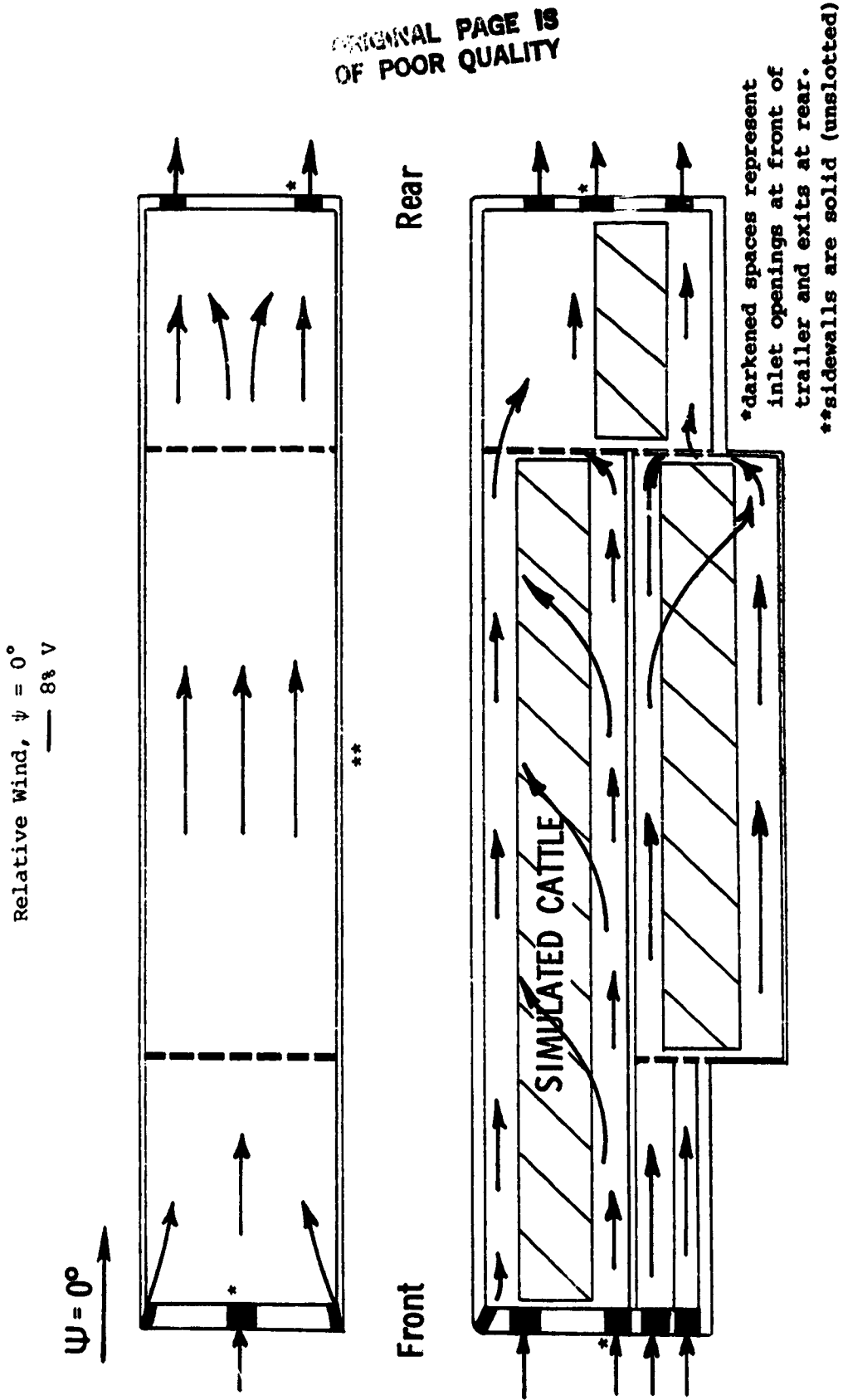


Figure 3.1.18 Air flow in trailer, $\Psi = 0^\circ$, configuration 6.

ORIGINAL PAGE IS
OF POOR QUALITY

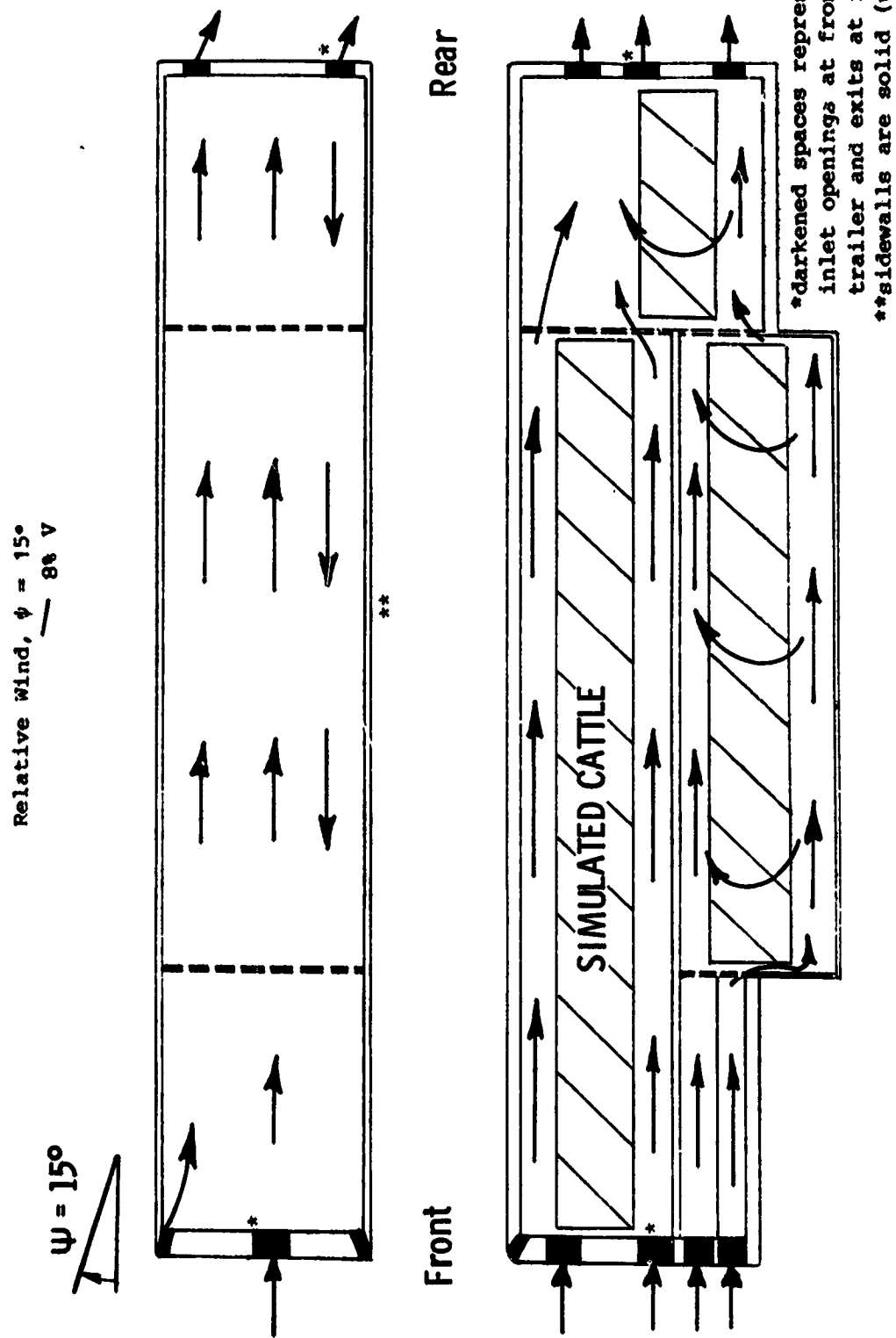


Figure 3.1.19 Air flow in trailer, $\psi = 15^\circ$, configuration 6.

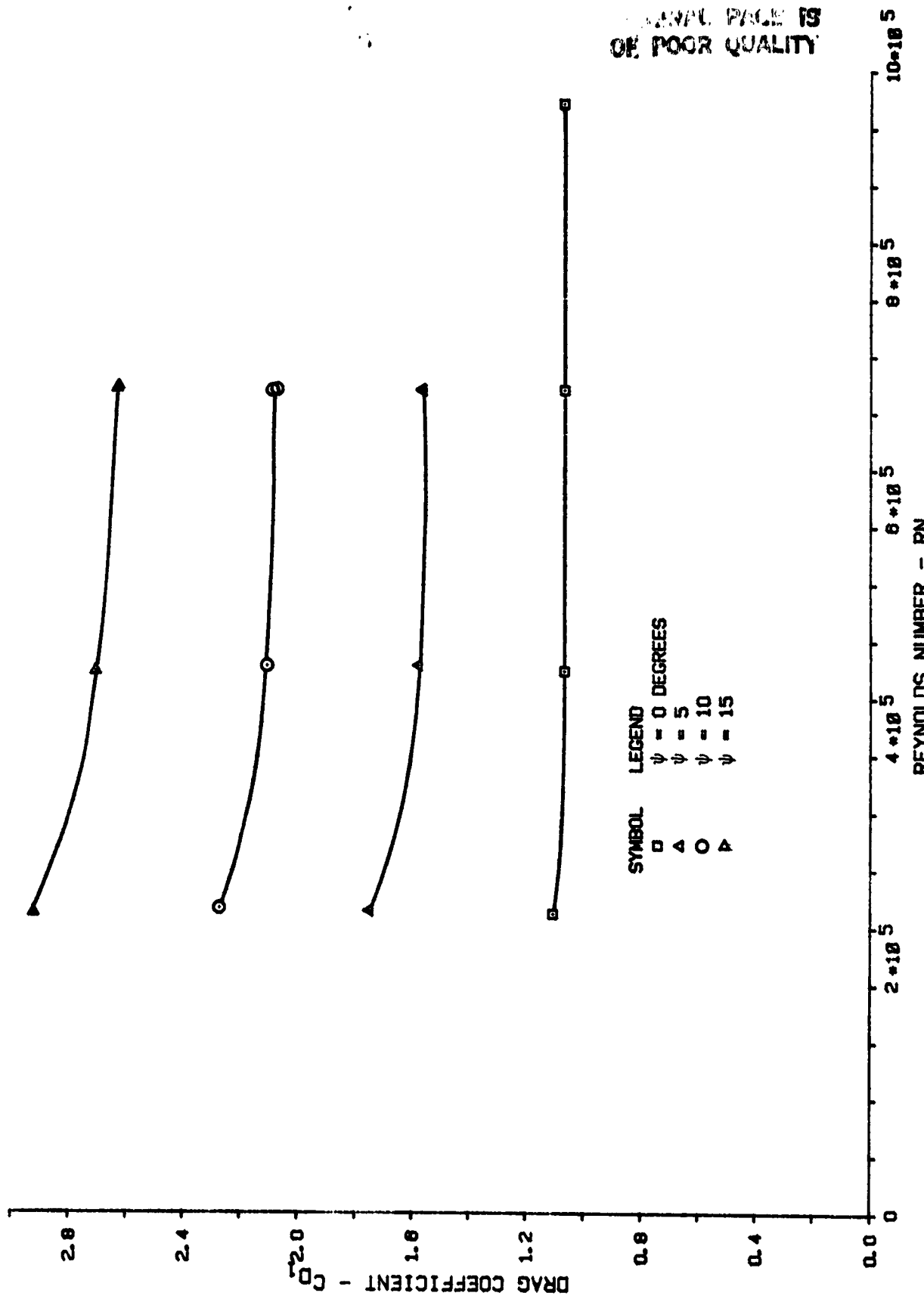


Figure 3.4.1 Reynolds number effect on drag coefficient, configuration 1.

ORIGINAL PAGE IS
OF POOR QUALITY

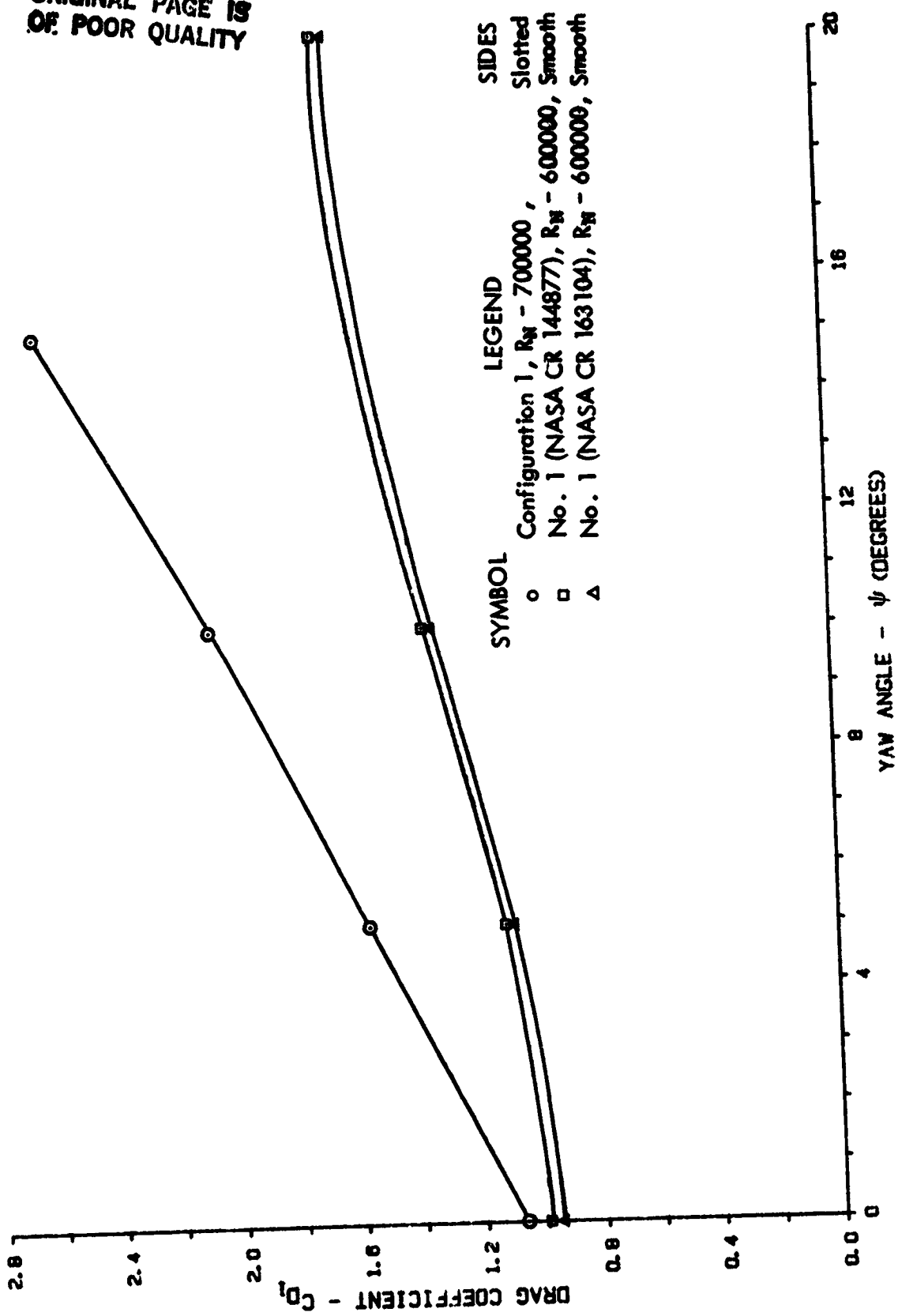


Figure 3.4.2 Effect of relative wind angle on drag coefficient, configuration 1.

Figure 3.4.2

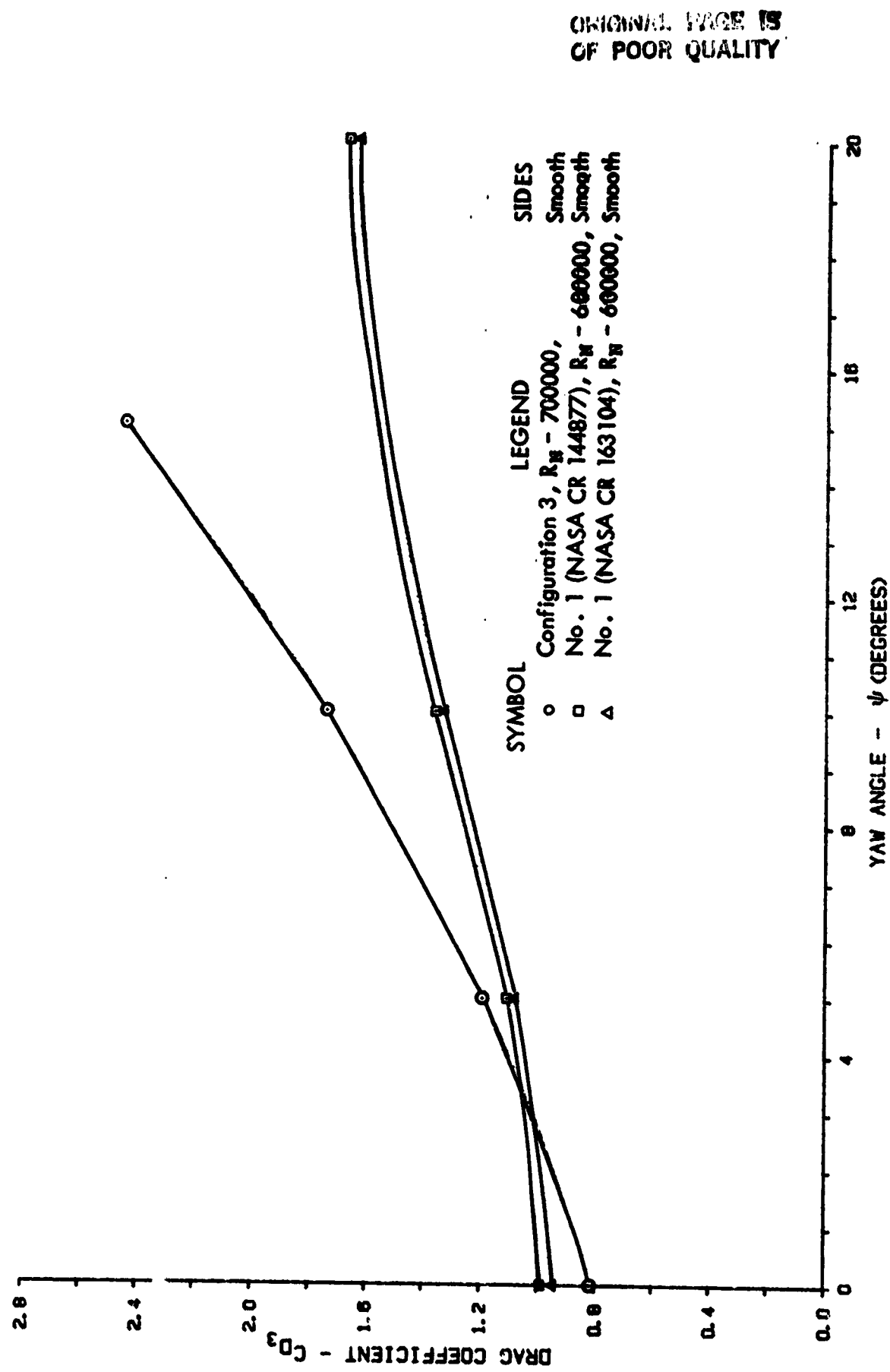


Figure 3.4.3 Effect of relative wind angle on drag coefficient, configuration 3.

ORIGINAL PAGE IS
OF POOR QUALITY

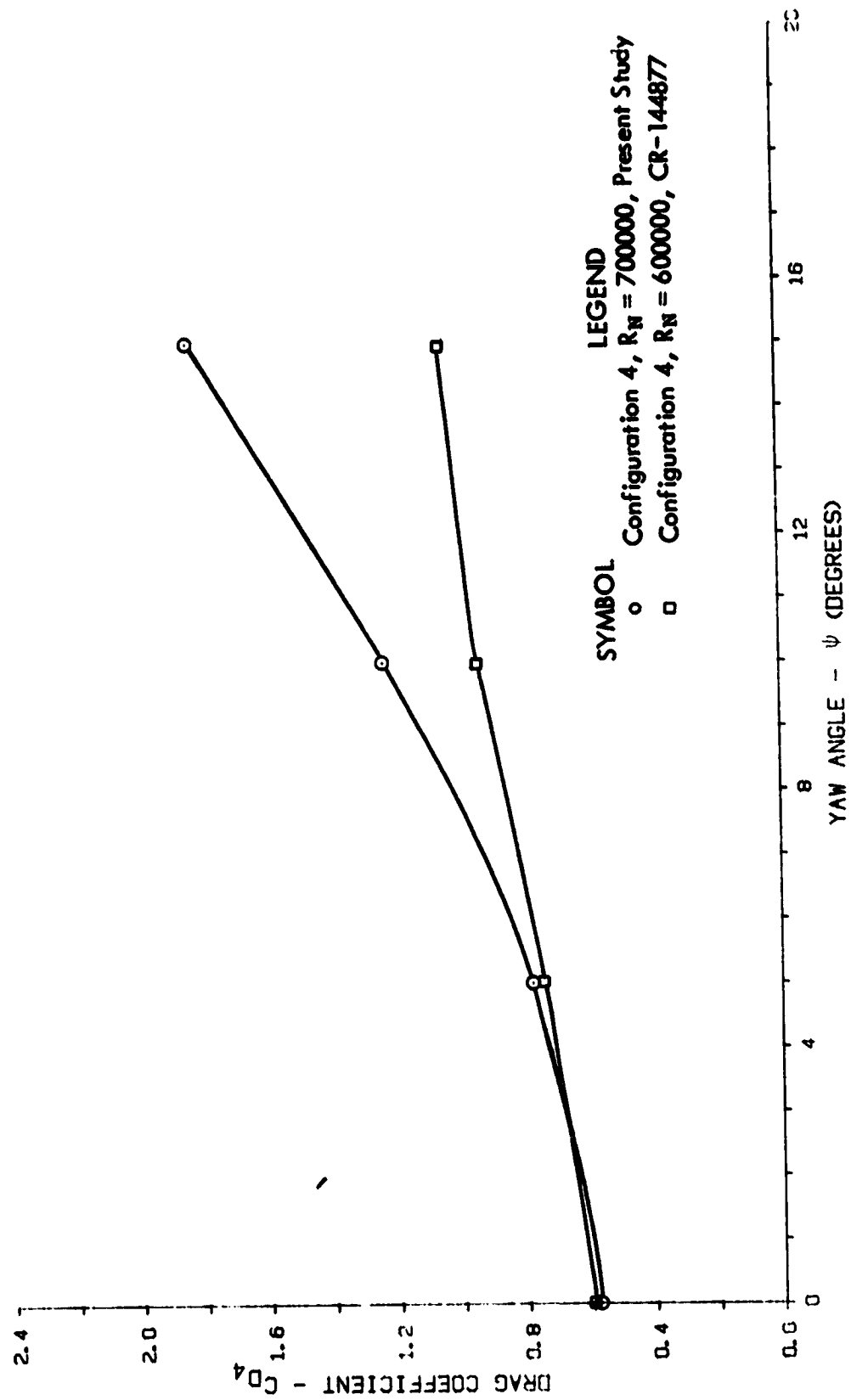


Figure 3.4.4 Effect of relative wind angle on drag coefficient, configuration 4.

ORIGINAL PAGE IS
OF POOR QUALITY

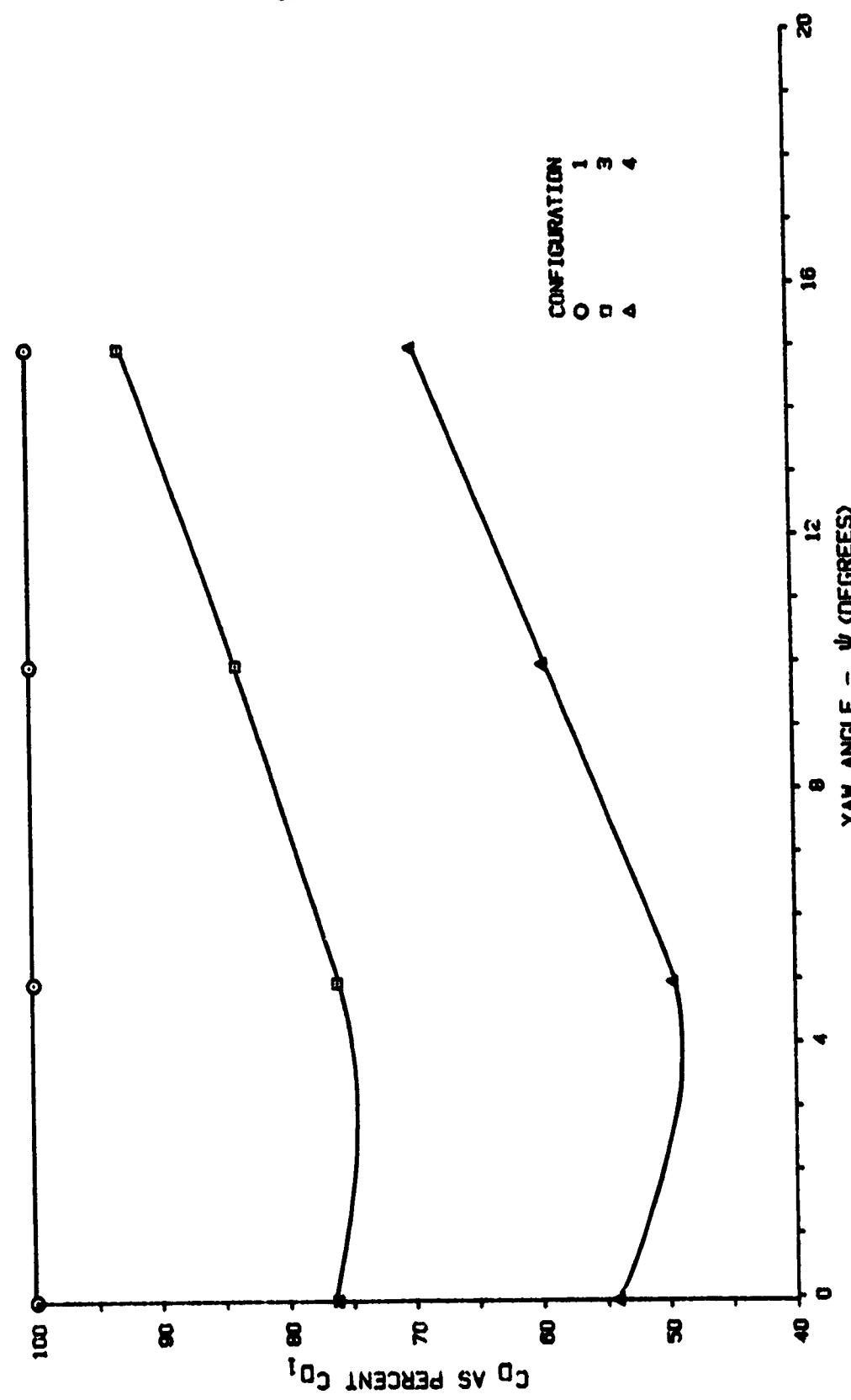


Figure 3.4.5 Comparison of drag coefficients, configurations 1, 3, 4.

ORIGINAL PAGE IS
OF POOR QUALITY

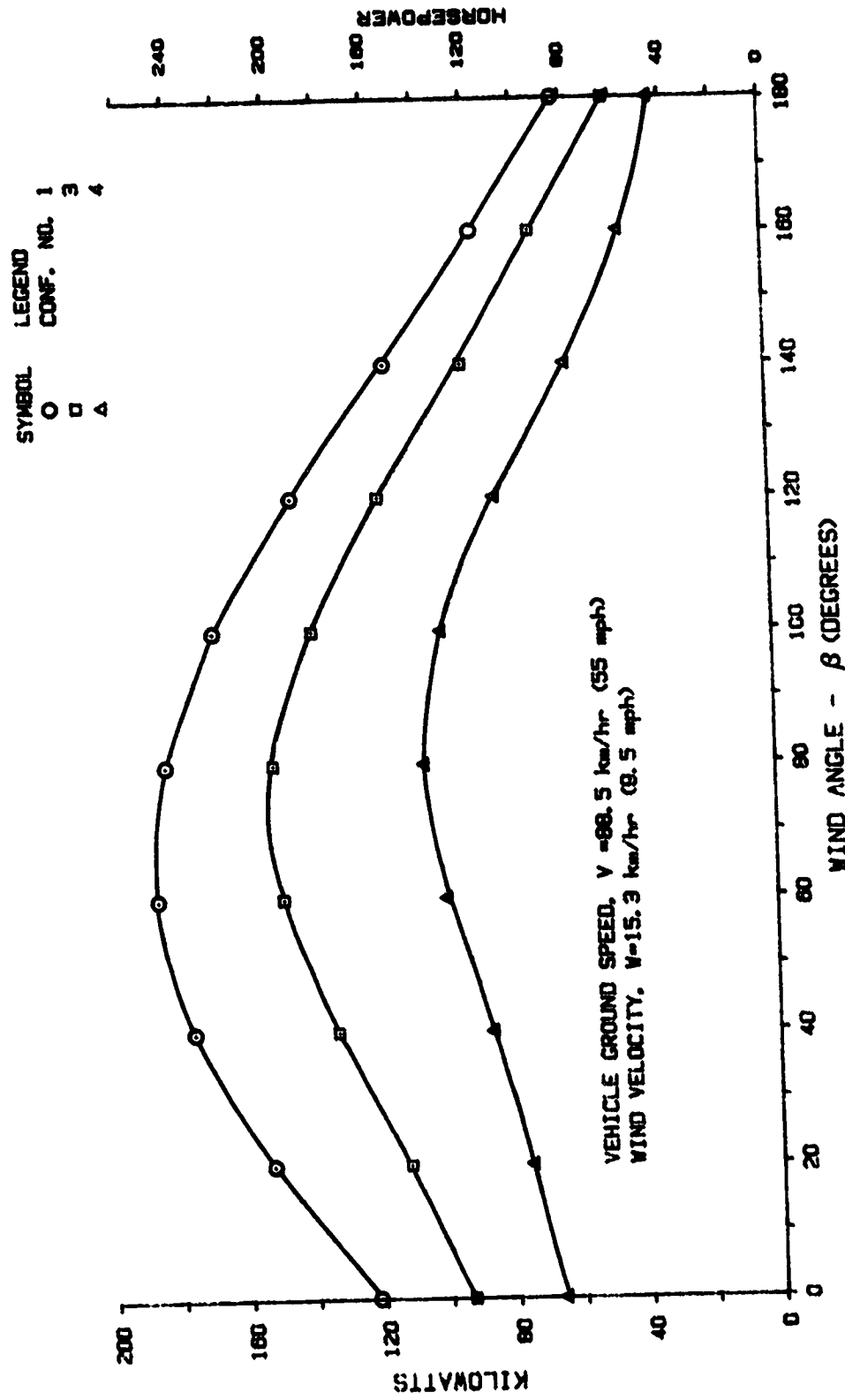


Figure 3.4.6 Power required to overcome aerodynamic drag, configurations 1, 3, 4.

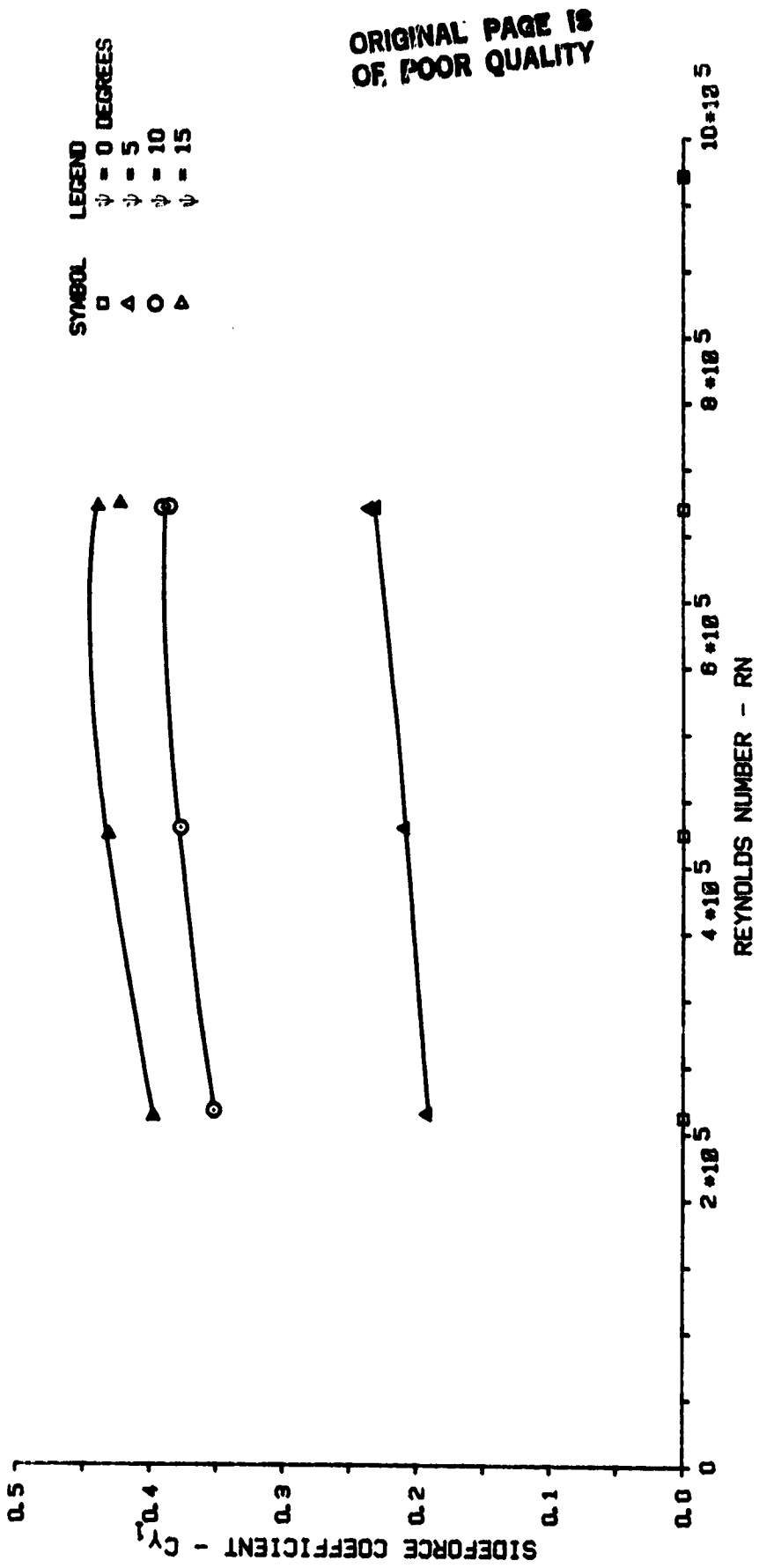


Figure 3.5.1 Reynolds number effect on side force coefficient, configuration 1.

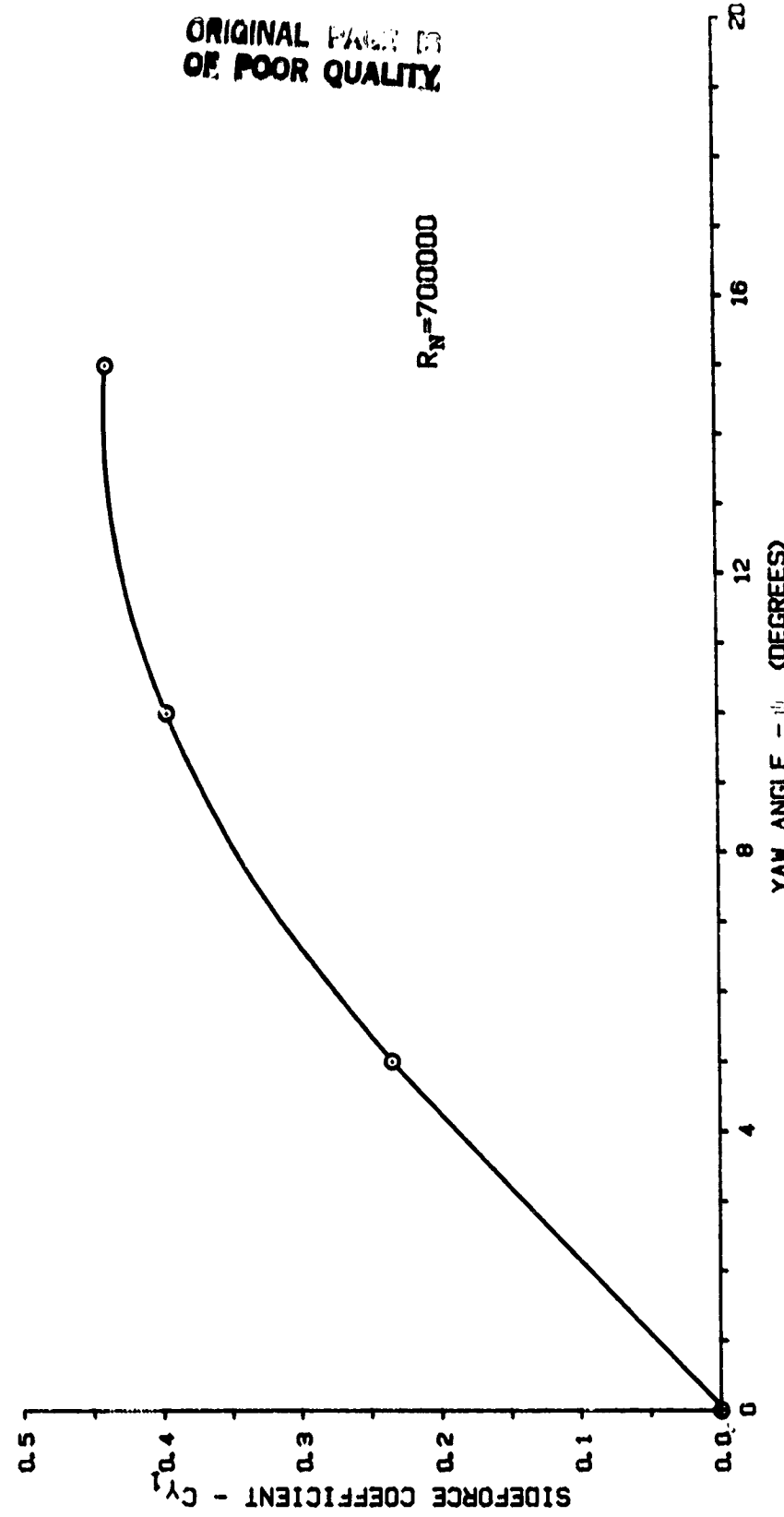


Figure 3.5.2 Effect of relative wind angle on side force coefficient, configuration 1.

ORIGINAL PAGE IS
OF POOR QUALITY

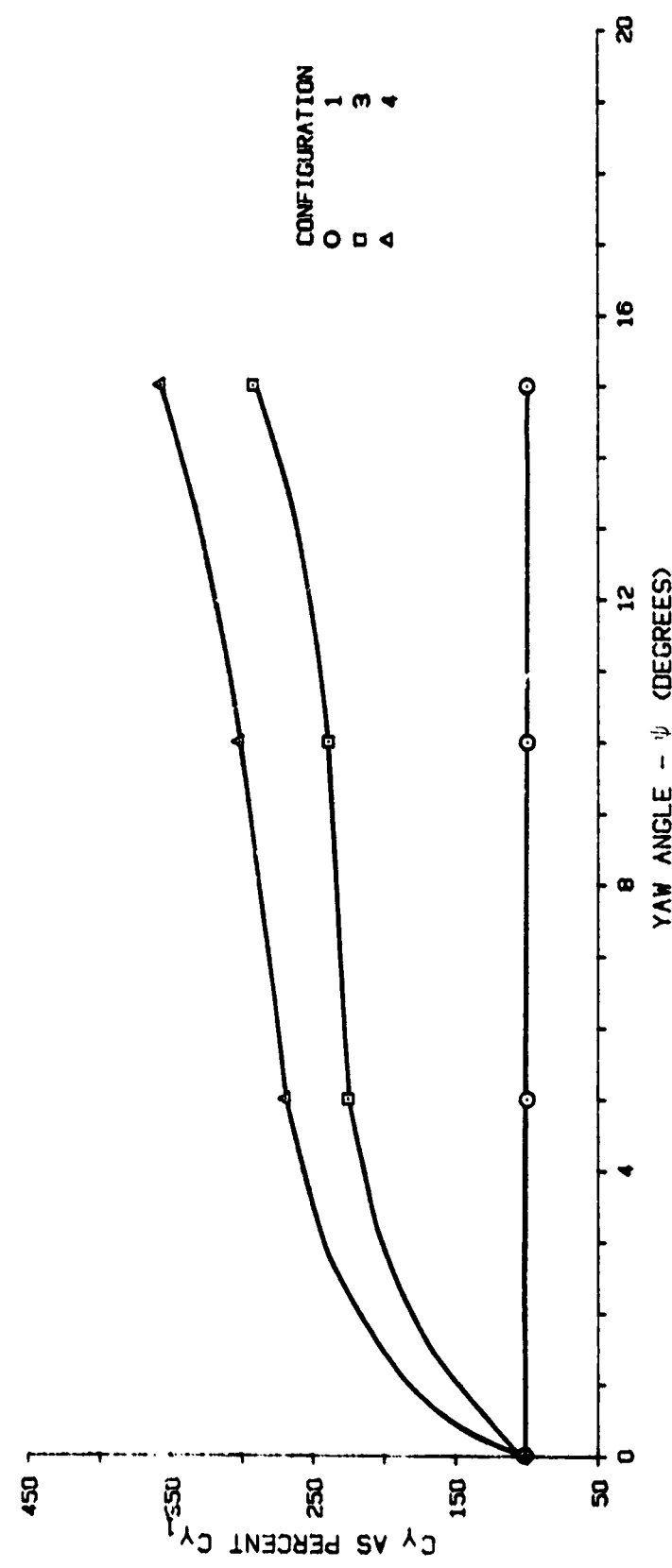


Figure 3.5.3 Comparison of side force coefficients, configurations 1, 3, 4.

ORIGINAL PAGE IS
OF POOR QUALITY

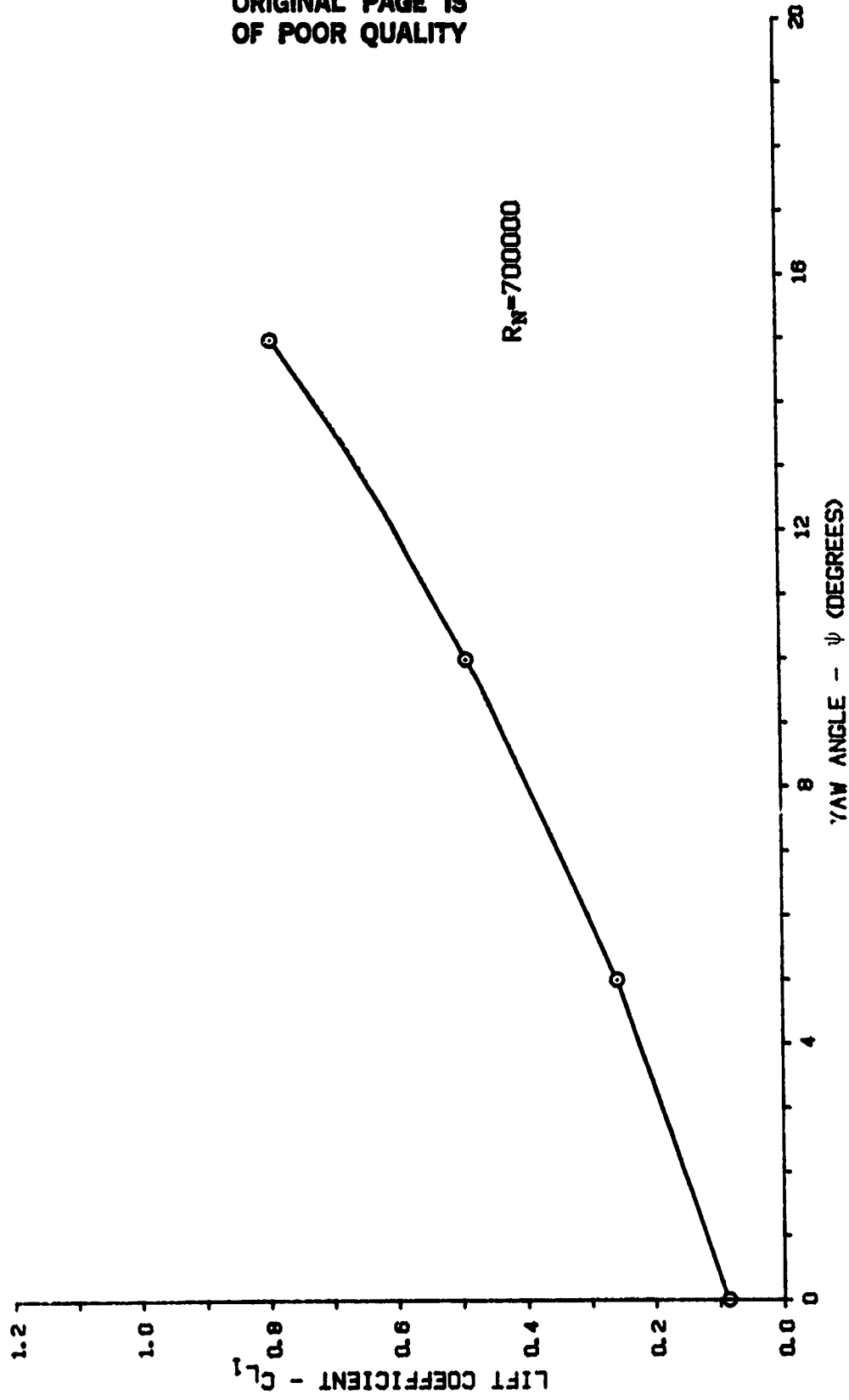


Figure 3.6.1 Effect of relative wind angle on lift coefficients, configuration 1.

ORIGINAL PAGE IS
OF POOR QUALITY

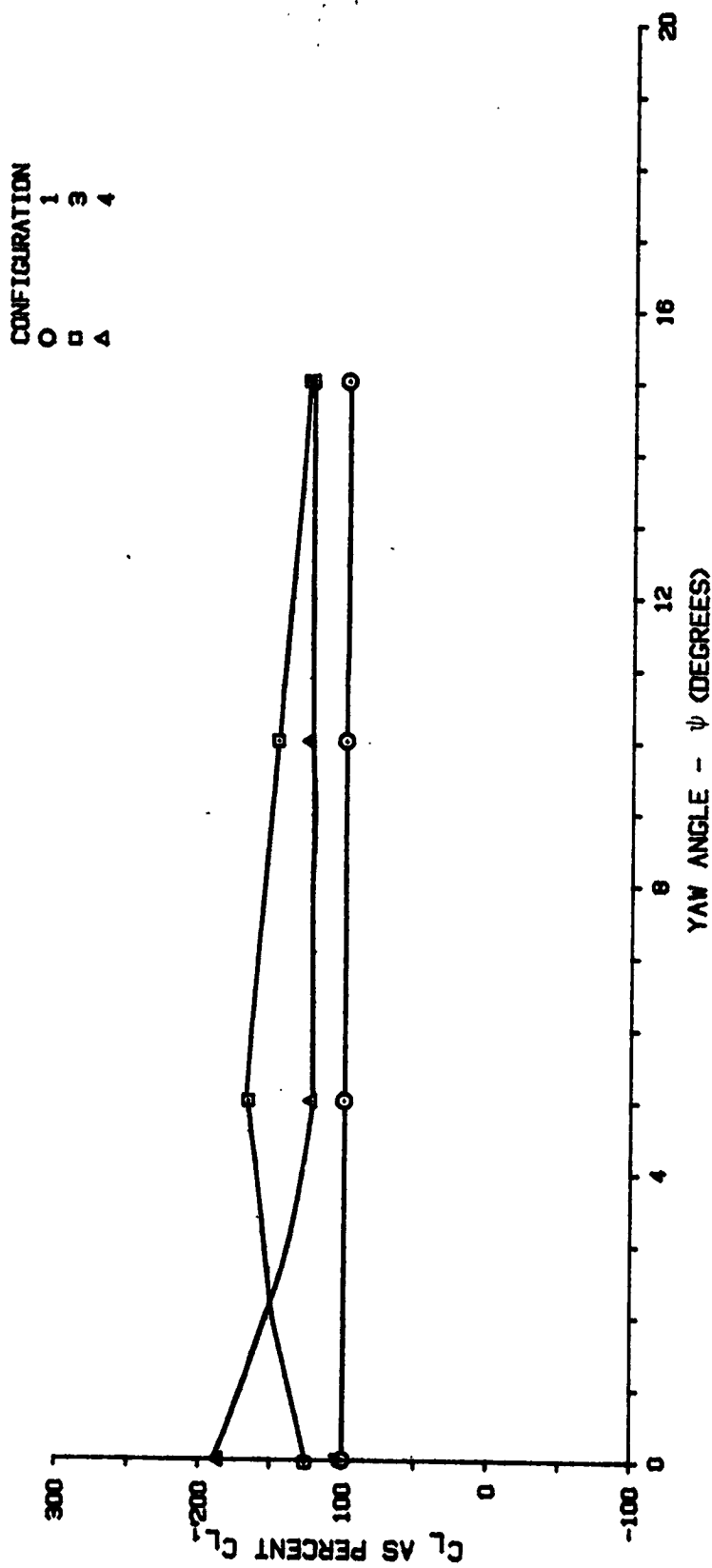


Figure 3.6.2 Comparison of lift coefficients, configurations 1, 3, 4.

ORIGINAL PAGE IS
OF POOR QUALITY

Table I. Coefficients of Static Pressure, Configuration 1

Yaw Angle, $\psi = 0^\circ$

$$R_N = 7.52 \times 10^5$$

Sides (outside)				Top (inside roof)					
Left		Right		Left		Center		Right	
Tap	C_p	Tap	C_p	Tap	C_p	Tap	C_p	Tap	C_p
7	-.184	40	-.121	2	-.223	1	-.106	30	-.094
12	-.143	45	-.046	61	-.082	60	-.094	6	-.094
15	-.136	48	-.046	64	-.082	63	-.059	62	-.059
10	-.053	43	-.053						
14	-.022	47	+.046						
8	-.015	41	-.075	67	-.094	66	-.082	65	-.035
21	-.106	54	-.113	31	-.070	32	-.070	68	-.082
25	-.121	58	-.143	71	-.059	70	-.047	69	-.047
28	-.121	5	+.060						
11	-.075	44	-.030	72	-.068	73	-.082	74	-.082
22	-.083	55	-.121	75	-.094	76	-.082	77	-.094
26	-.068	59	-.121						
9	-.046	42	-.068						
13	-.068	46	-.068	78	-.117	79	-.106	80	-.129
20	+.030	53	-.083	81	-.106	82	-.117	83	-.129
27	+.046	4	-.030	84	-.106	85	-.106	86	-.106
16	-.121	49	-.128	87	-.117	88	-.106	89	-.117
18	-.121	51	-.136						
23	-.121	56	-.143						
17	-.121	50	-.143	39	-.068	36	-.068	33	+.030
19	-.098	52	-.113	38	-.075	35	-.075	3	-.060
24	-.113	57	-.128	37	-.075	34	-.083	29	-.070

ORIGINAL PAGE IS
OF POOR QUALITY

Table I. Coefficients of Static Pressure, Configuration 1
Yaw Angle, $\psi = 5^\circ$ $R_N = 7.48 \times 10^5$

Sides (outside)				Top (inside roof)					
Left		Right		Left		Center		Right	
Tap	C_p	Tap	C_p	Tap	C_p	Tap	C_p	Tap	C_p
7	-.311	40	-.193	2	-.206	1	-.182	30	-.194
12	-.359	45	-.065	61	-.147	60	-.182	6	-.324
15	-.355	48	-.041	64	-.135	63	-.124	62	-.194
10	-.189	43	+.026	Upper Deck					
14	-.174	47	+.102	67	-.182	66	-.182	65	-.100
8	-.144	41	-.087	31	-.135	32	-.147	68	-.171
21	-.242	54	-.140	71	-.124	70	-.118	69	-.112
25	-.258	58	-.200	Front (inside)					
28	-.272	5	.000	72	-.174	73	-.171	74	-.159
11	-.174	44	-.019	75	-.182	76	-.171	77	-.171
26	-.174	59	-.079	Rear (inside)					
9	-.174	42	-.072	78	-.194	79	-.194	80	-.218
13	-.181	46	-.065	81	-.182	82	-.206	83	-.194
20	-.038	53	-.041	84	-.194	85	-.194	86	-.171
27	-.038	4	-.046	87	-.182	88	-.182	89	-.171
16	-.234	49	-.200	39	-.140	36	-.132	33	-.012
18	-.234	51	-.193	38	-.140	35	-.140	3	-.144
23	-.242	56	-.185	37	-.140	34	-.140	29	-.152
17	-.242	50	-.215						
19	-.196	52	-.193						
24	-.234	57	-.193						

**ORIGINAL PAGE IS
OF POOR QUALITY**

Table I. Coefficients of Static Pressure, Configuration 1

Yaw Angle, $\psi = 10^\circ$

$R_N = 7.42 \times 10^5$

Sides (outside)				Top (inside roof)					
Left		Right		Left		Center		Right	
Tap	C_p	Tap	C_p	Tap	C_p	Tap	C_p	Tap	C_p
7	-.454	40	-.198	2	-.291	1	-.338	30	-.314
12	-.462	45	-.023	61	-.279	60	-.303	6	-.457
15	-.454	48	-.023	64	-.208	63	-.184	62	-.267
10	-.293	43	+.114						
14	-.248	47	+.245						
8	-.248	41	-.061	67	-.291	66	-.327	65	-.184
21	-.324	54	-.160	31	-.208	32	-.270	68	-.243
25	-.317	58	-.176	71	-.160	70	-.160	69	-.220
28	-.332	5	+.004						
11	-.255	44	+.023	72	-.293	73	-.315	74	-.267
22	-.233	55	-.221	75	-.290	76	-.290	77	-.279
26	-.261	59	-.053						
9	-.271	42	-.084						
13	-.293	46	-.061	78	-.255	79	-.243	80	-.290
20	-.110	53	.000	81	-.232	82	-.290	83	-.196
27	-.088	4	-.026	84	-.243	85	-.243	86	-.220
16	-.317	49	-.260	87	-.232	88	-.232	89	-.230
18	-.317	51	-.252						
23	-.324	56	-.214						
17	-.340	50	-.290	39	-.183	36	-.176	33	-.031
19	-.29.	52	-.260	38	-.214	35	-.191	3	-.195
24	-.333	57	-.267	37	-.221	34	-.207	29	-.195

ORIGINAL PAGE IS
OF POOR QUALITY

Table I. Coefficients of Static Pressure, Configuration 1

Yaw Angle, $\psi = 15^\circ$

$$R_N = 7.42 \times 10^5$$

Sides (outside)				Top (inside roof)					
Left		Right		Left		Center		Right	
Tap	C_p	Tap	C_p	Tap	C_p	Tap	C_p	Tap	C_p
7	-.481	40	-.076	2	-.362	1	-.386	30	-.374
12	-.474	45	+.061	61	-.327	60	-.421	6	-.564
15	-.474	48	+.069	64	-.148	63	-.220	62	-.338
10	-.314	43	+.153						
14	-.352	47	+.450						
8	-.314	41	+.061	67	-.362	66	-.410	65	-.255
21	-.397	54	-.122	31	-.243	32	-.267	68	-.291
25	-.381	58	-.100	71	-.184	70	-.184	69	-.196
28	-.352	5	-.007						
11	-.352	44	+.061	72	-.357	73	-.386	74	-.338
22	-.328	55	-.191	75	-.362	76	-.374	77	-.350
26	-.357	59	-.015						
9	-.381	42	-.061						
13	-.397	46	-.038	78	-.303	79	-.291	80	-.350
20	-.254	53	+.046	81	-.255	82	-.327	83	-.220
27	-.167	4	.000	84	-.291	85	-.279	86	-.232
16	-.405	49	-.267	87	-.291	88	-.267	89	-.220
18	-.412	51	-.207						
23	-.428	56	-.167						
17	-.435	50	-.390	39	-.307	36	-.221	33	-.069
19	-.405	52	-.359	38	-.267	35	-.274	3	-.252
24	-.443	57	-.359	37	-.283	34	-.274	29	-.252

ORIGINAL PAGE IS
OF POOR QUALITY

Table II. Internal Air Flow Speeds, Configuration 2

Location	Yaw Angle, $\psi = 0^\circ$				
	Right		Middle		Left
A	7.9	(25.8)	-4.4	(-14.4)	Small (Small)
B	-3.4	(-11.3)	2.8	(9.2)	4.8 (15.9)
C	7.1	(23.4)	5.2	(17.2)	6.3 (20.6)
D	-3.4	(-11.2)	-2.0	(-6.5)	-2.0 (-6.5)
E	Small	(Small)	3.4	(11.3)	2.8 (9.2)
F	6.2	(20.6)	Small	(Small)	-2.8 (-9.2)

Location	Yaw Angle, $\psi = 5^\circ$				
	Right		Middle		Left
A	14.5	(47.5)	5.9	(19.5)	2.0 (6.5)
B	3.4	(11.3)	2.8	(9.2)	2.0 (6.5)
C	16.6	(54.4)	12.4	(40.6)	4.8 (15.9)
D	-2.0	(-6.5)	3.4	(11.3)	4.5 (14.9)
E	-2.0	(-6.5)	5.9	(19.5)	Small (Small)
F	2.0	(6.5)	Small	(Small)	-4.8 (-15.9)

Location	Yaw Angle, $\psi = 10^\circ$				
	Right		Middle		Left
A	24.9	(81.7)	15.1	(49.5)	8.2 (26.8)
B	3.4	(11.3)	Small	(Small)	-2.0 (-6.5)
C	22.1	(72.7)	17.7	(58.2)	2.0 (6.5)
D	4.8	(15.9)	7.4	(24.3)	2.8 (9.2)
E	4.4	(14.5)	7.4	(24.3)	-2.0 (-6.5)
F	4.4	(14.5)	-3.4	(-11.3)	-6.6 (-21.6)

Location	Yaw Angle, $\psi = 15^\circ$				
	Right		Middle		Left
A	24.0	(78.8)	17.9	(58.9)	9.1 (29.8)
B	13.6	(44.6)	8.9	(29.1)	-2.0 (-6.5)
C	13.4	(44.1)	22.3	(73.3)	2.0 (6.5)
D	5.9	(19.5)	9.6	(31.6)	2.0 (6.5)
E	3.4	(11.3)	7.1	(23.4)	4.0 (13.0)
F	6.2	(26.8)	-7.9	(-26.0)	-8.4 (-27.6)

Air flow speeds in meters/sec (ft/sec) with flow from front to rear positive

Small indicates air flow speed of less than .9 m/sec (3 ft/sec), positive or negative.

Wind tunnel airspeed 33.5 m/sec (110 ft/sec)

Table III. Internal Air Flow Speeds, Configuration 5

Location	Yaw Angle, $\psi = 0^\circ$			
	Right	Middle	Left	
A	4.4	(14.5)	5.9	(19.4)
B	2.0	(6.5)	5.6	(18.3)
C	5.2	(17.1)	3.4	(11.2)
D	3.4	'11.2)	2.8	(9.2)
E	4.0	(13.0)	3.4	(11.2)
F	4.0	(13.0)	2.8	(9.2)

Location	Yaw Angle, $\psi = 5^\circ$			
	Right	Middle	Left	
A	2.8	(9.2)	4.8	(15.9)
B	2.0	(5.5)	5.2	(17.1)
C	4.4	(14.5)	2.0	(6.5)
D	4.0	(13.0)	4.0	(13.0)
E	3.4	(11.2)	4.4	(14.5)
F	4.0	(13.0)	4.0	(13.0)

Location	Yaw Angle, $\psi = 10^\circ$			
	Right	Middle	Left	
A	4.0	(13.0)	4.8	(15.9)
B	2.0	(6.5)	6.2	(20.5)
C	4.0	(13.0)	4.0	(13.0)
D	2.0	(6.5)	2.8	(9.2)
E	2.8	(9.2)	4.0	(13.0)
F	3.4	(11.2)	3.4	(11.2)

Location	Yaw Angle, $\psi = 15^\circ$			
	Right	Middle	Left	
A	2.8	(9.2)	4.0	(13.0)
B	3.4	(11.2)	6.2	(20.5)
C	3.9	(12.9)	4.0	(13.0)
D	4.4	(14.5)	3.4	(11.2)
E	4.4	(14.5)	3.4	(11.2)
F	4.8	(15.9)	4.4	(14.5)

Air flow speeds in meters/sec (ft/sec) with flow from front to rear positive

Small indicates air flow speed of less than .9 m/sec (3 ft/sec), positive or negative.

Wind tunnel airspeed 33.5 /sec (110 ft/sec)

**ORIGINAL PAGE IS
OF POOR QUALITY**

Table IV. Internal Air Flow Speeds, Configuration 6

Location	Yaw Angle, $\psi = 0^\circ$					
	Right		Middle		Left	
A	2.8	(9.1)	2.8	(9.1)	2.8	(9.1)
B	Small	(Small)	Small	(Small)	Small	(Small)
C	2.0	(6.5)	2.0	(6.5)	2.8	(9.1)
D	2.0	(6.5)	2.0	(6.5)	3.4	(11.2)
E	2.0	(6.5)	2.8	(9.1)	Small	(Small)
F	2.0	(6.5)	2.0	(6.5)	2.0	(6.5)

Location	Yaw Angle, $\psi = 5^\circ$					
	Right		Middle		Left	
A	2.0	(6.5)	2.0	(6.5)	Small	(Small)
B	2.0	(6.5)	2.8	(9.1)	Small	(Small)
C	Small	(Small)	2.8	(9.1)	Small	(Small)
D	Small	(Small)	2.8	(9.1)	2.0	(6.5)
E	Small	(Small)	3.4	(11.2)	2.0	(6.5)
F	Small	(Small)	2.0	(6.5)	3.4	(11.2)

Location	Yaw Angle, $\psi = 10^\circ$					
	Right		Middle		Left	
A	2.8	(9.1)	2.0	(6.5)	Small	(Small)
B	3.4	(11.2)	2.0	(6.5)	Small	(Small)
C	Small	(Small)	2.0	(6.5)	-2.0	(-6.5)
D	2.0	(6.5)	4.0	(13.0)	-2.8	(-9.1)
E	Small	(Small)	3.4	(11.2)	2.0	(6.5)
F	2.8	(9.1)	2.8	(9.1)	2.0	(6.5)

Location	Yaw Angle, $\psi = 15^\circ$					
	Right		Middle		Left	
A	2.0	(6.5)	2.0	(6.5)	Small	(Small)
B	2.8	(9.1)	2.0	(6.5)	2.0	(6.5)
C	2.0	(6.5)	2.0	(6.5)	2.0	(6.5)
D	2.8	(9.1)	3.4	(11.2)	-2.0	(-6.5)
E	2.0	(6.5)	3.4	(11.2)	2.0	(6.5)
F	2.0	(6.5)	3.4	(11.2)	-2.0	(-6.5)

All air flow speeds in meters/sec (ft/sec) with flow from front to rear positive

Small indicates air flow speed of less than .9 m/sec (3 ft/sec), positive or negative

Wind tunnel airspeed 33.5 m/sec (110 ft/sec)

Table V. Internal Air Flow Volumes for Models

Number	Configuration				Yaw Angles, ψ	
	0°		5°		10°	15°
2 upper	.018	(.62)	.104	(3.69)	.169	(5.97)
2 lower	.110	(3.90)	.169	(5.96)	.240	(8.51)
Total	.128	(4.52)	.273	(9.65)	.409	(14.48)
5 upper	.089	(3.16)	.075	(2.66)	.091	(3.21)
5 lower	.076	(2.69)	.091	(3.21)	.081	(2.87)
Total	.165	(5.85)	.166	(5.87)	.172	(6.08)
6 upper	.028	(1.00)	.030	(1.05)	.035	(1.22)
6 lower	.060	(2.11)	.032	(1.13)	.013	(.47)
Total	.088	(3.11)	.062	(2.18)	.048	(1.69)

Volume, m^3/sec (ft^3/s)

Wind tunnel airspeed, 33.5 m/sec (110 ft/sec)

**ORIGINAL PAGE IS
OF POOR QUALITY**

**Table VI. Melting Times for Ice Cubes from Internal Air Flow,
Configuration 2**

Location	Yaw Angles, ψ			
	0°	5°	10°	15°
Test Section	2.2	2.2	2.2	2.2
A	2.4	5.6	5.6	5.4
B	8.5	4.9	6.2	3.4
C	6.5	4.3	4.2	4.1
D	8.0	4.6	5.3	5.5
E	14.3	8.6	8.3	8.5
F	12.6	10.2	7.4	7.3
G	4.8	4.5	5.5	4.4
H	5.4	5.2	5.0	6.6
I	1.6	2.5	2.7	7.0
J	1.6	2.2	2.3	3.8
K	9.7	6.2	8.7	7.1
L	1.9	1.9	2.1	2.5

All times in minutes and corrected to a tunnel test section temperature of 26.7°C (80°F)

Wind tunnel airspeed 33.5 m/sec (110 ft/sec)

**Table VII. Melting Times for Ice Cubes from Internal Air Flow,
Configuration 5**

Location	Yaw Angles, ψ			
	0°	5°	10°	15°
Test Section	2.2	2.2	2.2	2.2
A	5.4	6.1	5.8	5.8
B	6.6	8.6	10.3	12.0
C	7.6	9.9	11.5	10.3
D	8.8	9.8	8.5	8.6
E	5.8	7.3	7.4	9.5
F	7.9	7.8	6.9	8.1
G	4.2	3.4	5.0	7.7
H	9.8	11.9	14.1	11.7
I	11.5	9.1	10.5	14.8
J	10.4	9.5	12.1	14.8
K	14.4	11.7	19.0	17.0
L	4.1	4.3	3.8	3.9

All times in minutes and corrected to a tunnel test section temperature of 26.7°C (80°F)

Wind tunnel airspeed 33.5 m/sec (110 ft/sec)

Table VIII. Melting Times for Ice Cubes from Internal Flow,
Configuration 6

Location	Yaw Angles, ψ			
	0°	5°	10°	15°
Test Section	2.2	2.2	2.2	2.2
A	6.3	6.9	6.9	7.4
B	11.7	12.3	11.4	7.4
C	14.0	16.4	15.7	18.9
D	14.7	13.3	17.5	17.4
E	16.9	15.0	17.9	17.0
F	15.4	13.4	15.2	17.7
G	9.8	13.4	16.0	14.8
H	18.6	18.6	22.1	24.0
I	9.5	13.9	12.9	13.6
J	14.8	17.6	14.2	15.2
K	26.5	26.3	26.0	29.0
L	25.4	21.7	25.3	17.0

All times in minutes and corrected to a tunnel temperature of
26.7°C (80°F)

Wind tunnel air speed 33.5 m/sec (110 ft/sec)

Table IX. Drag Coefficients

Configuration	Yaw angles, ψ					Reynolds No.
	0°	5°	10°	15°	Average	
1	1.070	1.570	2.080	2.640	1.840	7×10^5
3	.816	1.195	1.743	2.448	1.550	7×10^5
4	.579	.778	1.239	1.838	1.109	7×10^5
No. 1 (NASA CR 144877)	.990	1.110	1.362	1.519*	1.245	6×10^5
No. 4 (NASA CR 144877)	.592	.750	.960	1.082*	.846	6×10^5
No. 5 (NASA CR 144877)	.506	.560	.646	.688*	.600	6×10^5

*Average of 10° and 20° data.

Table X. Potential Fuel and Economic Savings of Modified Vehicles Relative to Configurations 1 and 2¹

Configuration	Fuel quantity savings		Fuel Cost Savings	
	Liters (gal/hr) ²	Liters (gal) ³	\$/hr ⁴	\$ ^{3,4}
3	7.7 (2.0)	14,063 (3,740)	2.04	3,715
4, 5, 6	17.2 (4.5)	31,190 (8,240)	4.53	8,240

1 Vehicle speed 88.5 Km/hr (55 mph), annual national average winds 15.3 Km/hr (9.5 mph)

2 Brake specific fuel consumption = 2.129×10^{-4} kg of fuel per watt-hour (0.35 pounds per horsepower-hour) Diesel fuel density 0.834 kg/liter (6.96 lb/gal).

3 Assumed mileage - 160,900 Km per year (100,000 mi per year).

4 Assumed fuel cost = 26.4 cents per liter (1 dollar per gal.)

Table XI. Side Force Coefficients, $R_N = 7 \times 10^5$

Configuration	Yaw angles, ψ			
	0°	5°	10°	15°
1	.000	.235	.396	.438
3	.000	.511	.922	1.271
4	.000	.632	1.195	1.562
No. 1 (NASA CR 144877)	.000	.520	1.220	2.040*

*Average of 10° and 20° data

Table XII. Lift Coefficients, $R_N = 7 \times 10^5$

Configuration	Yaw Angles, ψ			
	0°	5°	10°	15°
1	.087	.258	.490	.790
3	.108	.442	.736	1.003
4	.162	.316	.612	.975

Table XIII. Pitching Moment Coefficients, $R_N = 7 \times 10^5$

Configuration	Yaw Angles, ψ			
	0°	5°	10°	15°
1	.004	.010	.027	.054
3	.006	.016	.039	.070
4	.008	.034	.059	.111

Table XIV. Rolling Moment Coefficients, $R_N = 7 \times 10^5$

Configuration	Yaw Angles, ψ			
	0°	5°	10°	15°
1	.000	-.001	-.005	-.200
3	.000	.017	-0.53	-.250
4	.000	-.049	-.158	-.324

Table XV. Yawing Moment Coefficients, $R_N = 7 \times 10^5$

Configuration	Yaw Angles, ψ			
	0°	5°	10°	15°
1	.000	-.065	-.550	-1.080
3	.000	-.820	-1.711	-2.342
4	.000	-1.495	-2.879	-4.133

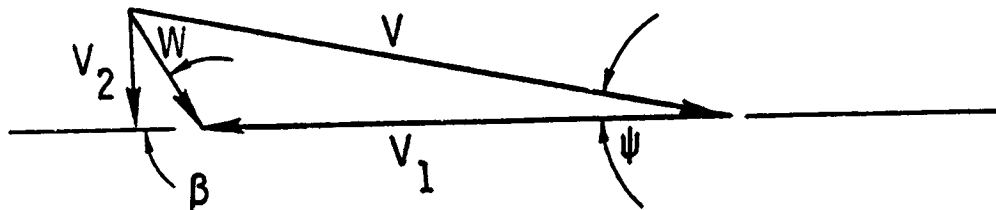
ORIGINAL PAGE IS
OF POOR QUALITY

7.0 APPENDIX

POWER REQUIRED

The model data for Configuration 1 were applied to the full size prototype vehicle at a road speed of 88.5 km/hr (55 mph). The wind component was rotated from 0° to 180°. The wind speed used was 15.3 km/hr (9.5 mph).

ORIGINAL PAGE IS
OF POOR QUALITY



v = Relative wind speed

v_1 = Ground speed

w = Actual wind velocity

v_2 = Side wind velocity component

β = Wind angle relative to the vehicle path

ψ = Relative wind angle

7.1 Power to Overcome Aerodynamic Drag - Configuration 1

The power required is:

$$P = \frac{D V_1}{1000} \text{ kw (Multiply by 1.341 = hp)}$$

ORIGINAL PAGE IS
OF POOR QUALITY

where

$$D = \frac{1}{2} \rho v^2 C_D A$$

A = 9.15 m² (98.6 ft²) - Full scale vehicle

$$\rho = 1.226 \text{ kg/m}^3 (.002378 \text{ slugs/ft}^3)$$

C_D is taken from Figure 3.4.2 for Configuration 1 at approximate values of ψ .

Example:

$$V_1 = 88.5 \text{ km/hr or } 24.58 \text{ m/sec (55 mph)}$$

$$W = 15.3 \text{ km/hr or } 4.25 \text{ m/sec (9.5 mph)}$$

$$\beta = 15^\circ$$

Relative wind angle:

$$\psi = \tan^{-1} \frac{W \sin \beta}{V_1 + W \cos \beta}$$

$$\psi = \tan^{-1} \frac{15.3 \text{ km/hr sin } 15^\circ}{88.5 \text{ km/hr} + 15.3 \text{ km/hr cos } 15^\circ}$$

$$\psi = 2.19^\circ$$

From Figure 3.4.2:

$$C_{D1} = 1.28$$

Then:

$$D = \frac{1}{2} \times 1.226 \times (28.71)^2 (1.28) (9.15)$$

$$D = 5917.8 \text{ N}$$

$$P = \frac{(5917.8) (24.58)}{1000} = 145.5 \text{ kw (195.1 hp)}$$